Photonic-Crystal Fibers

Philip St.J. Russell, *Member, IEEE*

Invited Paper

***Abstract*—The history, fabrication, theory, numerical modeling, optical properties, guidance mechanisms, and applications of photonic-crystal fibers are reviewed.**

***Index Terms*—Microstructured optical fibers, nonlinear optics, periodic structures, photonic band gaps (PBGs), photonic-crystal fibers (PCFs), waveguides.**

List of Acronyms

AS	Anti-Stokes.
ESM	Endlessly single mode.
FDTD	Finite-difference time domain.
GVD	Group velocity dispersion.
IR	Infrared.
MCVD	Modified chemical vapor deposition.
PBG	Photonic band gap.
PCF	Photonic-crystal fiber.
S	Stokes.
SC	Supercontinuum.
SMF	Single-mode fiber.
TIR	Total internal reflection.
WDM	Wavelength division multiplexing.

I. Introduction

PHOTONIC-CRYSTAL fibers (PCFs)—fibers with a periodic transverse microstructure—have been in practical existence as low-loss waveguides since early 1996 [1], [2]. The initial demonstration took four years of technological development, and since then, the fabrication techniques have become more and more sophisticated. It is now possible to manufacture the microstructure in air-glass PCF to accuracies of 10 nm on the scale of 1 μm, which allows remarkable control of key optical properties such as dispersion, birefringence, nonlinearity, and the position and width of the PBGs in the periodic "photonic-crystal" cladding. PCF has, in this way, extended the range of possibilities in optical fibers, both by improving well-established properties and introducing new features such as low-loss guidance in a hollow core.

Standard SMF, with a normalized core–cladding refractive-index difference[1] $\Delta \sim 0.4\%$, a core diameter of $\rho \sim 4.5$ μm, and, of course, very high optical clarity (better than 5 km/dB at 1550 nm), is actually quite limiting for many applications. Two major factors contribute to this. The first is the smallness of Δ, which causes bend loss (0.5 dB at 1550 nm in Corning SMF-28 for one turn around a mandrel 32 mm in diameter [3]) and limits the degree to which GVD and birefringence can be manipulated. Although much higher values of Δ can be attained (MCVD yields an index difference of 0.00146 per mol% GeO_2 up to a maximum $\Delta \sim 10\%$ for 100 mol% [4]), the single-mode core radius becomes very small, and the attenuation rises through increased absorption and Rayleigh scattering. The second factor is the reliance on TIR so that guidance in a hollow core is impossible, however useful it would be in fields requiring elimination of glass-related nonlinearities or enhancement of laser interactions with dilute or gaseous media. PCF has made it possible to overcome these limitations, and as a result, many new applications of optical fibers are emerging.

A. Outline of the Article

In Section II, a brief history of PCFs is given, and in Section III, fabrication techniques are reviewed. Numerical modeling and analysis are covered in Section IV and the optical properties of the periodic photonic-crystal cladding in Section V. The characteristics of guidance are discussed in Section VI (A: resonance and antiresonance; B and C: PCFs with positive and negative core–cladding index differences, respectively; D: birefringence; E: GVD; F: attenuation mechanisms; G: Kerr nonlinearities). In Section VII, many of the applications of PCFs are discussed (A: high-power transmission; B: lasers and amplifiers; C: intrafiber devices, cleaving, and splicing; D: Kerr-related nonlinear effects; E: Brillouin scattering; F: gas-based devices; G: telecommunications; H: laser tweezers; I: optical sensors), and some final remarks are made in Section VIII.

II. Brief History

The original motivation for developing PCFs was the creation of a new kind of dielectric waveguide—one that guides light by means of a two-dimensional (2-D) PBG. In 1991, the idea that the well-known "stopbands" in periodic structures [5] could be extended to prevent propagation in *all* directions [6] was leading to attempts worldwide to fabricate three-dimensional PBG materials. At that time, the received wisdom was that the refractive-index difference needed to create a PBG in two dimensions was large—of order 2.2 : 1. It was not widely recognized that the refractive-index difference requirements for

Manuscript received July 7, 2006; revised August 8, 2006.

The author is with the Max-Planck Research Group for Optics, Information, and Photonics, University of Erlangen-Nuremberg, 91058 Erlangen, Germany (e-mail: russell@optik.uni-erlangen.de).

Digital Object Identifier 10.1109/JLT.2006.885258

[1] $\Delta = (n_{\rm co} - n_{\rm cl})/n_{\rm cl}$, where $n_{\rm co}$ and $n_{\rm cl}$ are, respectively, the core and cladding refractive indices.

PBG formation in two dimensions are greatly relaxed if, as in a fiber, propagation is predominantly along the third axis—the direction of invariance.

A. PCFs

My idea, then, was to trap light in a hollow core by means of a 2-D "photonic crystal" of microscopic air capillaries running along the entire length of a glass fiber [7]. Appropriately designed, this array would support a PBG for incidence from air, preventing the escape of light from a hollow core into the photonic-crystal cladding and avoiding the need for TIR.

A question sometimes asked is whether these developments were really "new" or whether some aspects could be traced to previous work. While it is clear that no previous attempt had been made to produce photonic-crystal lattices of air holes in fiber form, or to create PBGs, there had been previous work on microstructured fibers. For example, in the 1970s, "single-component" fibers were investigated in which a central glass strand was held in place by two thin webs of glass [8]. This technology was rapidly abandoned with the introduction of MCVD. In the 1980s, in-fiber polarizers were developed at Southampton by drawing fibers with hollow side-channels ($\sim$30 μm in diameter) for introducing metal wires [9].

The first four years of work on understanding and fabricating PCF were a journey of exploration. Our first plan was to drill holes in a short rod of silica glass and then draw it down to fiber. Silica is a mechanically very hard material, and machining a large array of small holes in it proved beyond the capabilities of the tools available. In 1993, with funding from the Defence Research Agency in Malvern, U.K., work began in earnest, the initial idea being to adapt techniques widely used for the fabrication of multichannel image intensifier plates. These are made by stacking individual cylindrical elements into a 2-D close-packed array, the end result after drawing being a honeycomb of $\sim$10 μm diameter waveguide "pixels," each surrounded by black glass to reduce crosstalk. We also considered adapting techniques developed at the Naval Research Laboratory, Washington, DC, where cores from soluble glass, surrounded by insoluble glass, are arranged in a close-packed lattice and drawn down to microscopic dimensions. The soluble glass can then be dissolved out, leaving an array of tiny hollow channels in plates as thick as 200 μm [10], [11].

At this time, the parallel task of solving Maxwell's equations numerically was making good progress, culminating in a 1995 paper that showed that PBGs did indeed exist in 2-D silica–air structures for "conical" incidence from vacuum—this being an essential prerequisite for hollow-core guidance [12].

The first successful silica–air PCF structure was made in late 1995 by stacking 217 silica capillaries (eight layers outside the central capillary), specially machined with hexagonal outer cross sections and a circular inner cross section. The diameter-to-pitch ratio d/Λ of the holes in the final stack was $\sim$0.2, which theory showed was too small for PBG guidance in a hollow core, so we decided to make a PCF with a solid central core surrounded by 216 air channels [Fig. 1(a)] [1], [13], [14]. This led to the discovery of ESM PCF, which, if it guides at all, only supports the fundamental guided mode [15]. The success of these initial experiments led rapidly to a whole series of new types of PCF—large mode area [16], dispersion controlled [17], [18] hollow core [19], birefringent [20], and multicore [21].

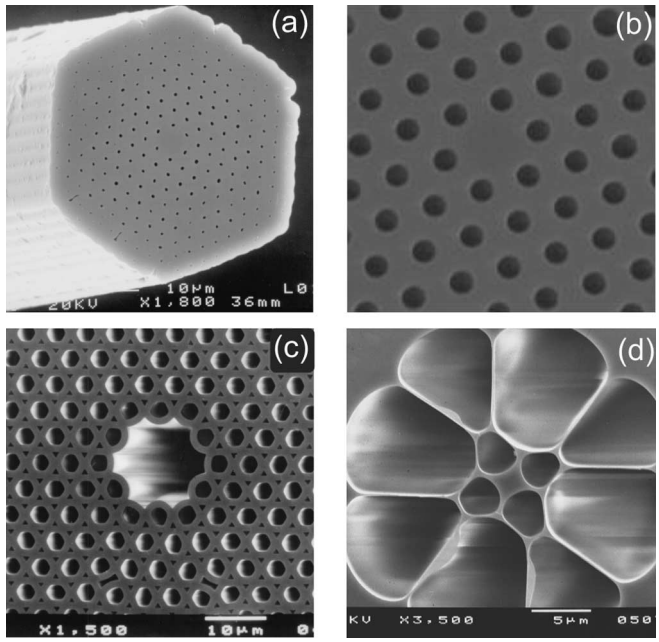

Fig. 1. Selection of scanning electron micrographs of PCF structures. (a) First working PCF—the solid glass core is surrounded by a triangular array of 300-nm-diameter air channels, spaced 2.3 μm apart [13], [14]. (b) Detail of a low-loss solid-core PCF (interhole spacing $\sim$2 μm). (c) First hollow-core PCF [19]. (d) PCF extruded from Schott SF6 glass with a core $\sim$2 μm in diameter [28].

These initial breakthroughs led quickly to applications, perhaps the most celebrated being the report in 2000 of SC generation from unamplified Ti:sapphire femtosecond laser pulses in a PCF with a core small enough to give zero dispersion at 800 nm wavelength (Section VII-D1) [22].

B. Bragg Fibers

In the late 1960s and early 1970s, theoretical proposals were made for another kind of fiber with a periodically structured cross section [23], [24]. This was a cylindrical "Bragg" fiber that confines light within an annular array of rings of high and low refractive index arranged concentrically around a central core. A group in France has made a solid-core version of this structure using MCVD [25]. Employing a combination of polymer and chalcogenide glass, researchers in the United States have realized a hollow-core version of a similar structure [26], reporting a 1-dB/m loss at the 10-μm wavelength (the losses at telecom wavelengths have yet to be specified). This structure guides light in the TE_{01} mode, which is used in microwave telecommunications because of its extremely low loss; the field moves away from the attenuating waveguide walls as the frequency increases, resulting in very low losses, although the guide must be kept very straight to avoid the fields entering the cladding and experiencing high absorption.

III. Fabrication Techniques

PCF structures are currently produced in many laboratories worldwide using a variety of different techniques (see Fig. 1

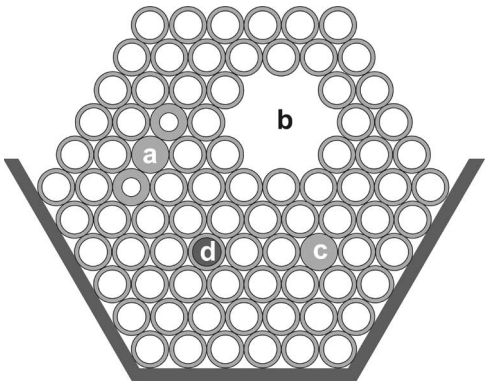

Fig. 2. Preform stack containing (a) birefringent solid core, (b) seven-cell hollow core, (c) solid isotropic core, and (d) doped core. The capillary diameters are ∼1 mm—large enough to ensure that they remain stiff for stacking.

for some example structures). The first stage is to produce a "preform"—a macroscopic version of the planned microstructure in the drawn PCF. There are many ways to do this, including stacking of capillaries and rods [13], [14] extrusion [27]–[30], sol–gel casting [31], injection molding, and drilling.

The most widely used technique is stacking of circular capillaries (Fig. 2). Typically, meter-length capillaries with an outer diameter of ∼1 mm are drawn from a starting tube of high-purity synthetic silica with a diameter of ∼20 mm. The inner/outer diameter of the starting tube, which typically lies in the range from 0.3 up to beyond 0.9, largely determines the d/Λ value in the drawn fiber. The uniformity in diameter and circularity of the capillaries must be controlled to at least 1% of the diameter. They are stacked horizontally in a suitably shaped jig to form the desired crystalline arrangement. The stack is bound with wire before being inserted into a jacketing tube, and the whole assembly is then mounted in the preform feed unit for drawing down to fiber. Judicious use of pressure and vacuum during the draw allows some limited control over the final structural parameters, for example, the d/Λ value.

Extrusion offers an alternative route to making PCF, or the starting tubes, from bulk glass; it permits formation of structures that are not readily made by stacking. While not suitable for silica (no die material has been identified that can withstand the ∼2000 °C processing temperatures without contaminating the glass), extrusion is useful for making PCFs from compound silica glasses, tellurites, chalcogenides, and polymers—materials that melt at lower temperatures. Fig. 1(d) shows the cross section of a fiber extruded, through a metal die, from a commercially available glass (Schott SF6) [28]. PCF has also been extruded from tellurite glass, which has excellent IR transparency out to beyond 4 μm, although the reported fiber losses (a few decibels per meter) are as yet rather high [30]. Polymer PCFs, which were first developed in Sydney, have been successfully made using many different approaches, for example, extrusion, casting, molding, and drilling [32].

A. Design Approach

The successful design of a PCF for a particular application is not simply a matter of using numerical modeling (see Section IV) to calculate the parameters of a structure that yields the required performance. This is because the fiber-drawing process is not lithographic but introduces its own highly reproducible types of distortion through the effects of viscous flow, surface tension, and pressure. As a result, even if the initial preform stack precisely mimics the theoretically required structure, several modeling and fabrication iterations are usually needed before a successful design can be reached.

IV. Modeling and Analysis

The complex structure of PCF—in particular, the large refractive-index difference between glass and air—makes its electromagnetic analysis challenging. Maxwell's equations must usually be solved numerically using one of a number of specially developed techniques [12], [33]–[36]. Although standard optical fiber analyses and a number of approximate models are occasionally helpful, these are only useful as rough guidelines to the exact behavior unless checked against accurate numerical solutions.

A. Maxwell's Equations

In most practical cases, a set of equal frequency modes is more useful than a set of modes of different frequency sharing the same value of axial wavevector component β. It is, therefore, convenient to arrange Maxwell's equations with β^2 as eigenvalue, i.e.,

$$\left(\nabla^2 + k^2\varepsilon(\mathbf{r}_T) + [\nabla \ln \varepsilon(\mathbf{r}_T)] \wedge \nabla\wedge\right)\mathbf{H}_T = \beta^2\mathbf{H}_T \quad (1)$$

where all the field vectors are taken in the form $\mathbf{Q} = \mathbf{Q}_T(\mathbf{r}_T)e^{-j\beta z}$, $\varepsilon_T(\mathbf{r}_T)$ is the dielectric constant, $\mathbf{r}_T = (x, y)$ is the position in the transverse plane, and $k = \omega/c$ is the vacuum wavevector. This form allows material dispersion to be easily included, which is something that is not possible if the equations are set up with k^2 as eigenvalue. Written out explicitly in Cartesian coordinates, (1) yields two equations relating h_x and h_y as follows:

$$\begin{aligned}\frac{\partial^2 h_x}{\partial y^2} + \frac{\partial^2 h_x}{\partial x^2} - \frac{\partial \ln\varepsilon}{\partial y}\left(\frac{\partial h_x}{\partial y} - \frac{\partial h_y}{\partial x}\right) + (\varepsilon k^2 - \beta^2)h_x = 0\\ \frac{\partial^2 h_y}{\partial x^2} + \frac{\partial^2 h_y}{\partial y^2} + \frac{\partial \ln\varepsilon}{\partial x}\left(\frac{\partial h_x}{\partial y} - \frac{\partial h_y}{\partial x}\right) + (\varepsilon k^2 - \beta^2)h_y = 0\end{aligned} \quad (2)$$

and a third differential equation relating h_x, h_y, and h_z, which is, however, not required to solve (2).

B. Scalar Approximation

In the paraxial scalar approximation, the second term inside the operator in (1), which gives rise to the middle terms in (2) that couple between the vector components of the field, can be neglected, yielding the following scalar wave equation:

$$\nabla^2\mathbf{H}_T + (k^2\varepsilon(\mathbf{r}_T) - \beta^2)\mathbf{H}_T = 0. \quad (3)$$

This leads to a scaling law similar to the one used in standard SMF analyses [38], which can be used to parameterize the fields

[39]. Defining Λ as the interhole spacing and n_1 and n_2 as the refractive indices of the two materials used to construct a particular geometrical shape of photonic crystal, the mathematical forms of the fields and the dispersion relations are identical, provided the generalized V-parameter defined by

$$V_{\mathrm{gen}} = k\Lambda\sqrt{n_1^2 - n_2^2} \tag{4}$$

is held constant. This has the interesting (though in the limit not exactly practical) consequence that band gaps can exist for vanishingly small index differences, provided the structure is made sufficiently large (see Section VI-C4).

C. Numerical Techniques

A common technique for solving (1) employs a Fourier expansion to create a basis set of plane waves for the fields, which reduces the problem to the inversion of a matrix equation suitable for numerical computation [34]. In contrast to the versions of Maxwell's equations with k^2 as eigenvalue [40], (1) is non-Hermitian, which means that standard matrix inversion methods cannot straightforwardly be applied. An efficient iterative scheme can, however, be used to calculate the inverse of the operator by means of fast Fourier transform steps. This method is useful for accurately finding the modes guided in a solid-core PCF, which are located at the upper edge of the eigenvalue spectrum of the inverted operator. In hollow-core PCF, however (or other fibers relying on a cladding band gap to confine the light), the modes of interest lie in the interior of the eigenvalue spectrum. A simple transformation can, however, be used to move the desired interior eigenvalues to the edge of the spectrum, greatly speeding up the calculations and allowing as many as a million basis waves to be incorporated [41], [42].

To treat PCFs with a central guiding core in an otherwise periodic lattice, a supercell is constructed, its dimensions being large enough so that once tiled, the guided modes in adjacent cores do not significantly interact. The plane-wave expansion method uses a Fourier series to represent the discontinuous dielectric function, so it suffers from the Gibb's phenomenon—the inability to accurately represent step changes. This introduces inaccuracy in the solutions that can usually (though not always, e.g., in high-index glass–air structures) be reduced by retaining more and more plane-wave components. A successful and accurate approach to alleviating this problem is to smooth out the sharp edges using super-Gaussian functions, though careful checks of the accuracy of the solutions must be carried out.

Other numerical techniques include expanding the field in terms of Hermite-Gaussian functions [42], [43], the use of FDTD analysis (a simple and versatile tool for exploring waveguide geometries [44]) and the finite-element approach [45]. If the PCF structure consists purely of circular holes, the multipole or Rayleigh method is a particularly fast and efficient method [36], [37]. It uses Mie theory to evaluate the scattering of the field incident on each hole. Yet another approach is a source-model technique that uses two sets of fictitious elementary sources to approximate the fields inside and outside circular cylinders [46].

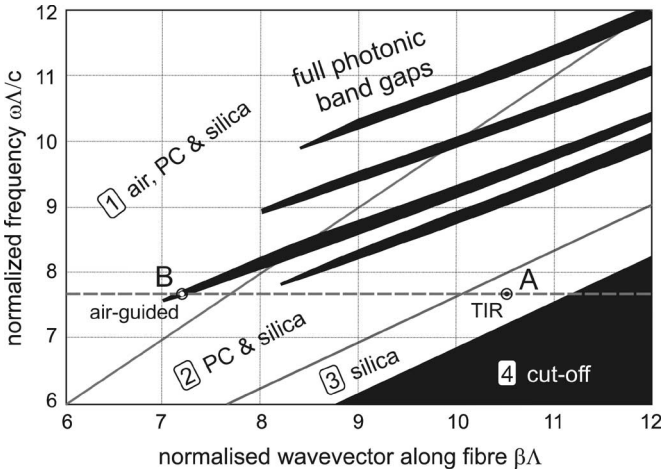

Fig. 3. Propagation diagram for a PCF with 45% air-filling fraction. Note the different regions where light is (1) able to propagate in all regions, (2) able to propagate also in the photonic-crystal cladding, (3) able to propagate only in silica glass, and (4) cut off completely. The "fingers" indicate the positions of full 2-D photonic band gaps [12].

V. Characteristics of Photonic-Crystal Cladding

The simplest photonic-crystal cladding is a biaxially periodic defect-free composite material with its own well-defined dispersion and band structure. These properties determine the behavior of the guided modes that form at cores (or "structural defects" in the jargon of photonic crystals). A convenient graphical tool is the propagation diagram—a map of the ranges of frequency and axial wavevector component β where light is evanescent in all transverse directions regardless of its polarization state (Fig. 3) [12]. The vertical axis is the normalized frequency $k\Lambda$, and the horizontal axis is the normalized axial wavevector component $\beta\Lambda$. Light is unconditionally cut off from propagating (due to either TIR or a PBG) in the black regions.

In any subregion of isotropic material (i.e., glass or air) at fixed optical frequency, the maximum possible value of $\beta\Lambda$ is given by $k\Lambda n$, where n is the refractive index (at that frequency) of the region under consideration. For $\beta < kn$, light is free to propagate, for $\beta > kn$, it is evanescent, and at $\beta = kn$, the critical angle is reached, denoting the onset of TIR for light incident from a medium of index larger than n.

The slanted guidelines (Fig. 3) denote the transitions from propagation to evanescence for air, the photonic crystal, and glass. At fixed optical frequency for $\beta < k$, light propagates freely in every subregion of the structure. For $k < \beta < kn_{\mathrm{g}}$, in which n_{g} is the index of the glass, light propagates in the glass substrands and is evanescent in the hollow regions. Under these conditions, the "tight binding" approximation holds, and the structure may be viewed as an array of coupled glass waveguides.

A. Maximum Refractive Index

The maximum axial refractive index $n_{\max} = \beta_{\max}/k$ in the photonic-crystal cladding lies in the range $k < \beta < kn_{\mathrm{g}}$ as expected of a composite glass–air material. This value coincides with the z-pointing "peaks" of the dispersion surfaces in

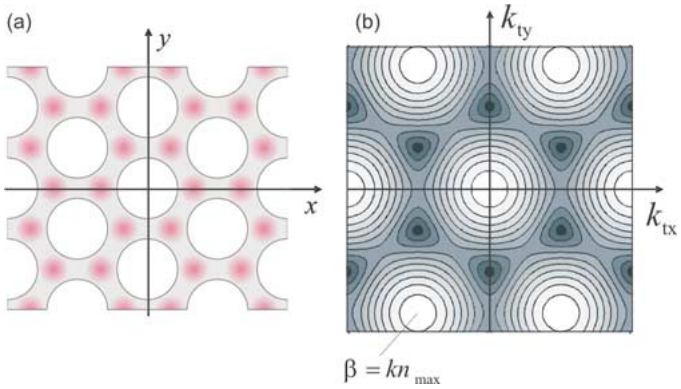

Fig. 4. (a) Real-space schematic of the tight-binding picture of modes guided in the glass substrands in a triangular array of air holes. Each substrand couples to three neighbors, and by applying Bloch's theorem, the allowed values of transverse wavevector may be calculated at fixed β and k. (b) Reciprocal space picture of the dispersion surfaces for increasing values of β. At a particular value of β, a passband opens up (the dark-shaded triangular features) and the field amplitudes change sign between adjacent substrands. As β increases, the passband is traversed, terminating at a maximum value (corresponding to $n_{\max}$) where the field amplitudes in all substrands have the same sign.

reciprocal space, where multiple values of transverse wavevector are allowed, one in each tiled Brillouin zone. For a constant value of β slightly smaller than $\beta_{\max}$, these wavevectors lie on small approximately circular loci, with a transverse component of group velocity that points normal to the circles in the direction of increasing frequency (Fig. 4). Thus, light can travel in *all* directions in the transverse plane, even though its wavevectors are restricted to values lying on the circular loci.

Thus, $n_{\max}$ depends strongly on frequency, even though neither the air nor the glass is assumed dispersive in the analysis; microstructuring itself creates dispersion through a balance between transverse energy storage and energy flow that is highly dependent upon frequency.

By averaging the square of the refractive index in the photonic-crystal cladding, it is simple to show that

$$n_{\max} \to \sqrt{(1-F)n_{\rm g}^2 - Fn_a^2}, \qquad k\Lambda \to 0 \tag{5}$$

in the long-wavelength limit for a scalar approximation, where F is the air-filling fraction, and n_a is the index in the holes, which we take to be equal to 1 in what follows.

As the wavelength of the light falls, the optical fields are better able to distinguish between the glass regions and the air. The light piles up more and more in the glass, causing the effective $n_{\max}$ "seen" by it to change. In the limit of small wavelength $k\Lambda \to \infty$, light is strongly excluded from the air holes by TIR, and the field profile "freezes" into a shape that is independent of wavelength. The variation of $n_{\max}$ with frequency may be estimated by expanding fields centered on the air holes in terms of Bessel functions and applying symmetry [15]. Defining the normalized parameters

$$u = \Lambda\sqrt{k^2 n_{\rm g}^2 - \beta^2}, \quad v = k\Lambda\sqrt{n_{\rm g}^2 - 1} \tag{6}$$

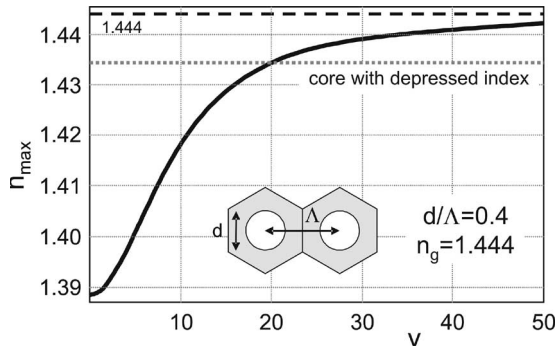

Fig. 5. Maximum axial refractive index in the photonic-crystal cladding as a function of the normalized frequency parameter v for $d/\lambda = 0.4$ and $n_g = 1.444$. For this filling fraction of air (14.5%), the value at long wavelength ($v \to 0$) is $n_{\max} = 1.388$, which is in agreement with (5). The horizontal dashed gray line represents the case when the core is replaced with a glass of refractive index $n_{\rm co} = 1.435$ (below that of silica) when guidance ceases for $v > 20$.

the analysis yields the following polynomial fit (see the Appendix):

$$u(v) = (0.00151 + 2.62v^{-1} + 0.0155v - 0.000402v^2 + 3.63 \times 10^{-6}v^3)^{-1} \tag{7}$$

for $d/\Lambda = 0.4$ and $n_{\rm g} = 1.444$. This polynomial is accurate to better than 1% in the range $0 < v < 50$. The resulting expression for $n_{\max}$ is plotted in Fig. 5 against the parameter v.

B. Transverse Effective Wavelength

The transverse effective wavelength in the ith material is defined as follows:

$$\lambda_{\rm eff}^i = \frac{2\pi}{\sqrt{k^2 n_i^2 - \beta^2}} \tag{8}$$

where n_i is its refractive index. This wavelength can be many times the vacuum value, tends to infinity at the critical angle $\beta \to kn_i$, and is imaginary when $\beta > kn_i$. It is a measure of whether or not the light is likely to be resonant within a particular feature of the structure, for example, a hole or a strand of glass, and defines PCF as a wavelength-scale structure.

C. PBGs

Full 2-D PBGs exist in the black finger-shaped regions in Fig. 3. Some of these extend into the region $\beta < k$, where light is free to propagate in vacuum, confirming the feasibility of trapping light within a hollow core.

The band gap edges coincide with points where resonances in the cladding unit cells switch on and off, i.e., the eigenvalues of the unitary inter-unit-cell field transfer matrices change from $\exp(\pm j\phi)$ (propagation) to $\exp(\pm\gamma)$ (evanescence). At these transitions, depending on the band edge, the light is to a greater or lesser degree preferentially redistributed into the low- or high-index subregions. For example, at fixed optical frequency and small values of β, leaky modes peaking in the low-index channels form a passband that terminates when the standing wave pattern has 100% visibility. For the high-index strands

(Fig. 4), on the other hand, the band of real states is bounded by a lower value of β where the field amplitude changes sign between selected pairs of adjacent strands, depending on the lattice geometry, and an upper bound where the field amplitude does not change sign between the strands (this field distribution yields $n_{\max}$).

VI. Characteristics of Guidance

In SMF, guided modes form within the range of axial refractive indices $n_{\rm cl} < n_z < n_{\rm co}$ when light is evanescent in the cladding ($n_z = \beta/k$; core and cladding indices are represented by $n_{\rm co}$ and $n_{\rm cl}$). In PCF, three distinct guidance mechanisms exist, namely 1) a modified form of TIR [15], [47], 2) PBG guidance [19], [48], and 3) a leaky mechanism based on a low density of photonic states in the cladding [49]. In the following subsections, we explore the role of resonance and antiresonance and discuss chromatic dispersion, attenuation mechanisms, and guidance in cores with refractive indices raised and lowered relative to the "mean" cladding value.

A. Resonance and Antiresonance

It is helpful to view the guided modes as being confined (or not confined) by resonance and antiresonance in the unit cells of the cladding crystal. If the core mode finds no states in the cladding with which it is phase-matched, light cannot leak out. This is a familiar picture in many areas of photonics. What is perhaps not so familiar is the use of the concept in two dimensions, where a repeating unit is tiled to form a photonic-crystal cladding. This allows the construction of an intuitive picture of "cages," "bars," and "windows" for light and actually leads to a blurring of the distinction between guidance by modified TIR and PBG effects.

B. Positive Core–Cladding Index Difference

This type of PCF may be defined as one where the mean cladding refractive index in the long-wavelength limit $k \to 0$ (5) is lower than the core index (in the same limit). Under correct conditions (high air-filling fraction), PBG guidance may also occur in this case, although experimentally, the TIR-guided modes will dominate.

1) Controlling the Number of Modes: A striking feature of this type of PCF is that it is "ESM," i.e., the core does not become multimode in the experiments no matter how short the wavelength of the light [15]. Although the guidance in some respects resembles conventional TIR, it turns out to have some interesting and unique features that distinguish it markedly from step-index fiber. These are due to the piecewise discontinuous nature of the core boundary—sections where, for $n_z > 1$, air holes that strongly block the escape of light are interspersed with regions of barrier-free glass. In fact, the cladding operates in a regime where the transverse effective wavelength (8) in silica is comparable with the glass substructures in the cladding. The zone of operation in Fig. 3 is $n_{\max} < n_z < n_{\rm g}$ (point A).

In a solid-core PCF, taking the core radius $\rho = \Lambda$ and using the analysis in [15], the effective V-parameter can be calculated. This yields the plot in Fig. 6, where the full behavior from very low to very high frequency is predicted. As expected, the number of guided modes $\sim V_{\rm PCF}^2/2$ is almost independent of wavelength at high frequencies; the single-mode behavior is determined solely by the geometry. Numerical modeling shows that if $d/\Lambda < 0.43$, the fiber never supports any higher order guided modes, i.e., it is ESM.

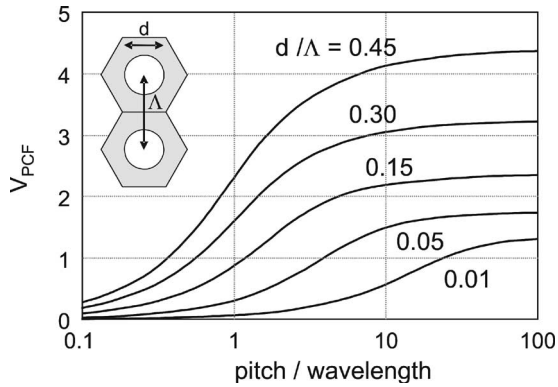

Fig. 6. V-parameter for solid-core PCF (triangular lattice) plotted against the ratio of hole spacing to vacuum wavelength for different values of d/Λ. Numerical modeling shows that ESM behavior is maintained for $V_{\rm PCF} \leq 4$ or $d/\Lambda \leq 0.43$.

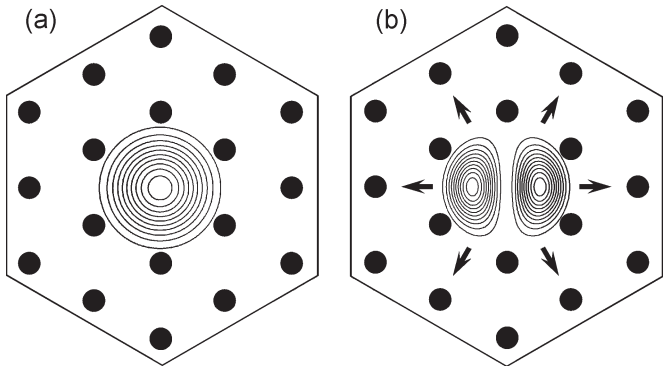

Fig. 7. Modal filtering in a solid-core PCF. (a) Fundamental mode is trapped. (b) Higher order modes leak away through the gaps between the air holes.

This behavior can be understood by viewing the array of holes as a modal filter or "sieve" (Fig. 7). The fundamental mode in the glass core has a transverse effective wavelength $\lambda_{\rm eff}^{\rm g} \approx 4\Lambda$. It is, thus, unable to "squeeze through" the glass channels between the holes, which are $\Lambda - d$ wide and, thus, below the Rayleigh resolution limit $\approx \lambda_{\rm eff}^{\rm g}/2 = 2\Lambda$. Provided the relative hole size d/Λ is small enough, higher order modes are able to escape—their transverse effective wavelength is shorter, so they have higher resolving power. As the holes are made larger, successive higher order modes become trapped.

ESM behavior may also be viewed as being caused by strong wavelength dispersion in the photonic-crystal cladding, which forces the core–cladding index step to fall as the wavelength gets shorter (Fig. 5) [15], [47]. This counteracts the usual trend toward increasingly multimode behavior at short wavelengths. In the limit of very short wavelength, the light strikes the glass–air interfaces at glancing incidence and is strongly rejected from the air holes. In this regime, the transverse single-mode

profile does not change with wavelength. Consequently, the angular divergence (roughly twice the numerical aperture) of the emerging light is proportional to wavelength—in SMFs, it is approximately constant due to the appearance of more and more higher order guided modes as the frequency increases.

Thus, the refractive index of the photonic-crystal cladding increases with optical frequency, tending toward the index of silica glass in the short-wavelength limit. If the core is made from a glass of refractive index lower than that of silica (e.g., fluorine-doped silica), guidance is lost at wavelengths shorter than a certain threshold value (see Fig. 5) [50]. Such fibers have the unique ability to prevent transmission of short-wavelength light—in contrast to conventional fibers that guide more and more modes as the wavelength falls.

2) Ultra-Large-Area Single Mode: The modal filtering in ESM-PCF is controlled only by the geometry (e.g., d/Λ for a triangular lattice). A corollary is that the behavior is quite independent of the absolute size of the structure, permitting SMF cores with arbitrarily large areas. A single-mode PCF with a core diameter of 22 μm at 458 nm was reported in 1998 [16]. In conventional step-index fibers, where $V < 2.405$ for single-mode operation, this would require uniformity of core refractive index to $\sim$1 part in 10^5—very difficult to achieve if MCVD is used to form the doped core. Larger mode areas allow higher power to be carried before the onset of intensity-related nonlinearities or damage and have obvious benefits for delivery of high laser power, fiber amplifiers, and fiber lasers. The bend-loss performance of such large-core PCFs is discussed in Section VI-B.

3) Fibers With Multiple Cores: The stacking procedure makes it straightforward to produce multicore fiber. A preform stack is built up with a desired number of solid (or hollow) cores and drawn down to fiber in the usual manner [21]. The coupling strength between the cores depends on the sites chosen, because the evanescent decay rate of the fields changes with azimuthal direction. Applications include curvature sensing [51]. More elaborate structures can be built up such as fibers with a central single-mode core surrounded by a highly multimode cladding waveguide and are useful in applications such as high-power cladding-pumped fiber lasers [52] and two-photon fluorescence sensors [53] [see Section VII-B and Fig. 8(j)].

4) Nanoweb Fibers: The stacking and drawing procedure also makes it possible to produce some quite unusual structures such as a "nanoweb" fiber [Fig. 8(b)]. Somewhat similar to the single-component fibers from the 1970s [8], it does not have a deliberately introduced core but instead relies on a gentle thickness gradient to confine the light. The glass web can be as narrow as 200 nm and as long as 100 μm. The extremely low loss (0.4 dB/m) in what is essentially a planar glass waveguide with very strong waveguide dispersion makes this an interesting structure for experiments in spatial solitons and nonlinear optics [54].

C. Negative Core–Cladding Index Difference

Since TIR cannot operate under these circumstances, low-loss waveguiding is only possible if a PBG exists in the range $\beta < k\, n_{\rm core}$.

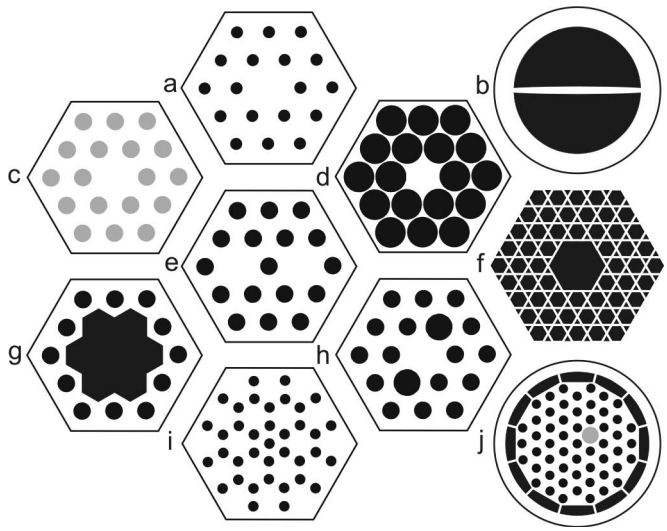

Fig. 8. Representative sketches of different types of PCF. The black regions are hollow, the white regions are pure glass, and the gray regions are doped glass. (a) ESM solid-core PCF. (b) Nanoweb fiber (not a PCF). (c) All-solid-glass PCF with raised-index doped glass strands (colored gray) in the cladding. (d) SC PCF (with high air-filling fraction and small core). (e) Dual-core PCF. (f) Kagomé hollow-core PCF. (g) Seven-cell hollow-core PCF. (h) Birefringent PCF. (i) Carbon-ring structure for PBG guidance. (j) Double-clad PCF with offset doped lasing core and high numerical aperture inner cladding for pumping (the photonic-crystal cladding is held in place by thin webs of glass).

1) Hollow-Core Silica–Air: In a silica–air PCF, larger air-filling fractions and small interhole spacings are necessary to achieve PBGs in the region $\beta < k$. The relevant operating region in Fig. 3 is to the left of the vacuum line and inside one of the band gap fingers (point B). These conditions ensure that light is free to propagate and form guided modes within the hollow core while being unable to escape into the cladding. The number N of such modes is controlled by the depth and width of the refractive-index "potential well" and is approximately given by

$$N \approx k^2 \rho^2 \left(n_{\rm high}^2 - n_{\rm low}^2\right)/2 \tag{9}$$

where $n_{\rm high}$ and $n_{\rm low}$ are the refractive indices at the edges of the PBG at fixed frequency, and ρ is the core radius. Since the band gaps are quite narrow ($n_{\rm high}^2 - n_{\rm low}^2$ is typically a few percent), the hollow core must be sufficiently large if a guided mode is to exist at all. In the first hollow-core PCF reported in 1999 [19], the core was formed by omitting seven capillaries from the preform stack [Fig. 1(c)]. An electron micrograph of a more recent structure, with a hollow core made by removing 19 missing capillaries from the stack, is shown in Fig. 9 [55].

In hollow-core PCF, guidance can only occur when a PBG coincides with a core resonance. This means that only restricted bands of wavelength are guided. This feature can be very useful for suppressing parasitic transitions by filtering away the unwanted wavelengths, for example, in fiber lasers and in stimulated Raman scattering in gases (see Section VII-F1).

2) Glass of Higher Refractive Index: Achieving a band gap in glasses of higher refractive index for $\beta < k$ presents, at first glance, a dilemma. Whereas a larger refractive-index contrast generally yields wider band gaps, the higher "mean" refractive index seems likely to make it more difficult to achieve band

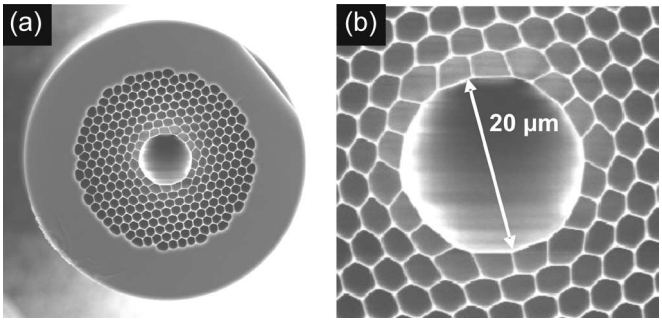

Fig. 9. (a) Example of a low-loss hollow-core PCF (fabricated by BlazePhotonics Ltd.). The core diameter is 20.4 μm, and the attenuation in the best cases approaches 1 dB/km at 1550 nm wavelength. (b) Detail of the core region.

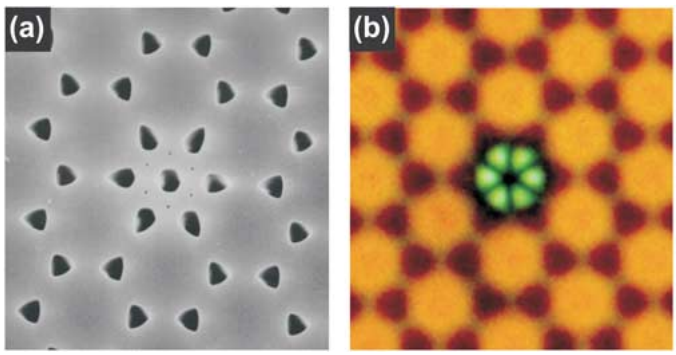

Fig. 10. (a) PCF with a "carbon-ring" lattice of air holes and an extra central hole to form a low-index core. (b) When white light is launched, only certain bands of wavelength are transmitted in the core—here, a six-lobed green mode emerges from the end-face (near-field image) [48].

gaps for incidence from vacuum. Although this argument holds in the scalar approximation, the result of calculations show that vector effects become important at higher levels of refractive-index contrast (e.g., 2 : 1 or higher), and a new species of band gap appears for smaller filling fractions of air than in silica-based structures. The appearance of this new type of gap means that it is actually easier to make hollow-core PCFs from glasses of higher index such as tellurites or chalcogenides [41].

3) Surface States on Core–Cladding Boundary: The first PCF that was guided by PBG effects consisted of a lattice of air holes arranged in the same way as the carbon rings in graphite. The core was formed by introducing an extra hole at the center of one of the rings, with its low index precluding the possibility of TIR guidance [48]. When white light was launched into the core region, a colored mode was transmitted—the colors being dependent on the absolute size to which the fiber was drawn. The modal patterns had six equally strong lobes that are disposed in a flower-like pattern around the central hole. Closer examination revealed that the light was guided not in the air holes but in the six narrow regions of glass surrounding the core (Fig. 10). The light remained in these regions, despite the close proximity of large "rods" of silica, full of modes. This is because for particular wavelengths, the phase velocity of the light in the core is not coincident with any of the phase velocities available in the transmission bands created by nearest neighbor coupling between rod modes. Light is, thus, unable to couple over to them and remains trapped in the core. This

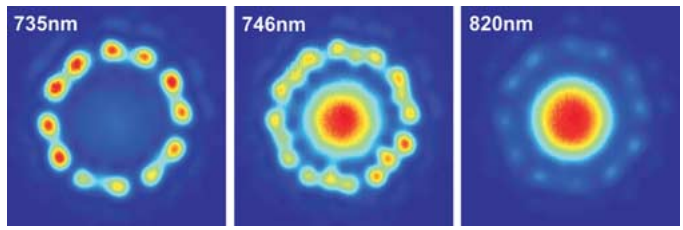

Fig. 11. Near-field end-face images of the light transmitted in hollow-core PCF designed for 800 nm transmission. For light launched in the core mode, at 735 nm, a pure surface mode is transmitted, at 746 nm, a coupled surface-core mode is transmitted, and at 820 nm, a pure core mode is transmitted (false-color images courtesy G. Humbert, University of Bath) [59].

mechanism of PBG formation can only operate in extended one-dimensional (1-D) or 2-D structures (modes trapped within defect layers in multilayer stacks show the same behavior [56]).

Similar guided modes are commonly seen in hollow-core PCF, where they form surface states (analogous with electronic surface states in semiconductor crystals) on the rim of the core, confined on the air side by TIR and on the cladding side by PBG effects. These surface states become phase-matched to the air-guided mode at certain wavelengths (Fig. 11), creating couplings (anticrossings on the frequency-wavevector diagram) that perturb the GVD and contribute additional attenuation (see Section VI-A) [57]–[59].

4) All-Solid Structures: In all-solid band gap guiding fibers, the core is made from low-index glass and is surrounded by an array of high-index glass strands [60], [61]. Since the mean core–cladding index contrast is negative, TIR cannot operate, and PBG effects are the only possible guidance mechanism. These structures have some similarities with 1-D "ARROW" structures, where antiresonance plays an important role [62].

When the cladding strands are antiresonant, light is confined to the central low-index core by a mechanism not dissimilar to the modal filtering picture in Section II-A; the high-index cores act as the "bars of a cage" so that no features in the cladding are resonant with the core mode, resulting in a low-loss guided mode. Guidance is achieved over wavelength ranges that are punctuated with high-loss windows where the cladding "bars" become resonant (Fig. 12). Remarkably, it is possible to achieve PBG guidance by this mechanism even at index contrasts of 1% [61], [63], with losses as low as 20 dB/km at 1550 nm [64].

5) Low-Density-of-States Guidance: The transmission bands are greatly widened in hollow-core PCFs with a Kagomé lattice in the cladding [49] [Fig. 8(f)]. Fig. 13 shows the attenuation spectrum of such a fiber, the minimum loss being $\sim$1 dB/m over a bandwidth of several hundred nanometers. Numerical simulations show that while the cladding structure supports no band gaps, the density of states is greatly reduced near the vacuum line. The consequential poor overlap between the core states, together with the greatly reduced number of cladding states, slows down the leakage of light but does not completely prevent it.

D. Birefringence

The modes of a perfect sixfold symmetric core and cladding structure are not birefringent [65]. In practice, however, the

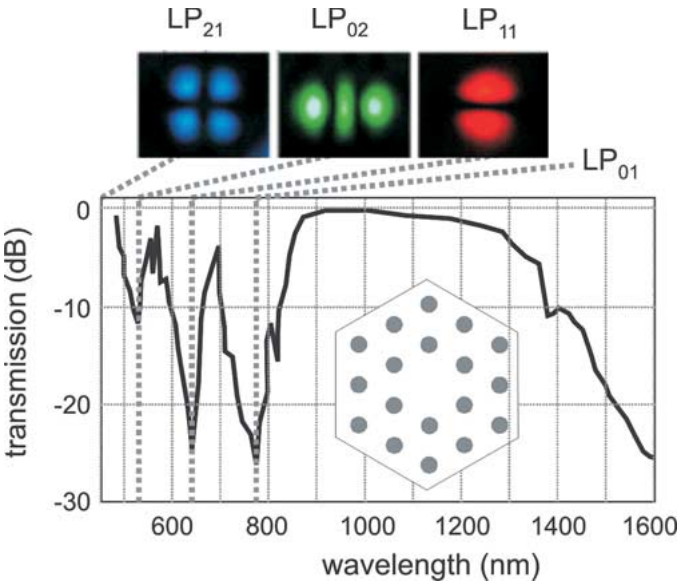

Fig. 12. Lower: Measured transmission spectrum (using a white-light SC source) for a PCF with a pure silica core and a cladding formed by an array of Ge-doped strands ($d/\Lambda = 0.34$, hole spacing $\sim$7 μm, index contrast 1.05 : 1). The transmission is strongly attenuated when the core mode becomes phase-matched to different LP_{nm} "resonances" in the cladding strands. Upper: Experimental images [taken with blue (500 nm), green (550 nm), and red (650 nm) filters] of the near-field profiles in the cladding strands at three such wavelengths. The fundamental LP_{01} resonance occurs at $\sim$820 nm, and the four-lobed blue resonance lies off the edge of the graph.

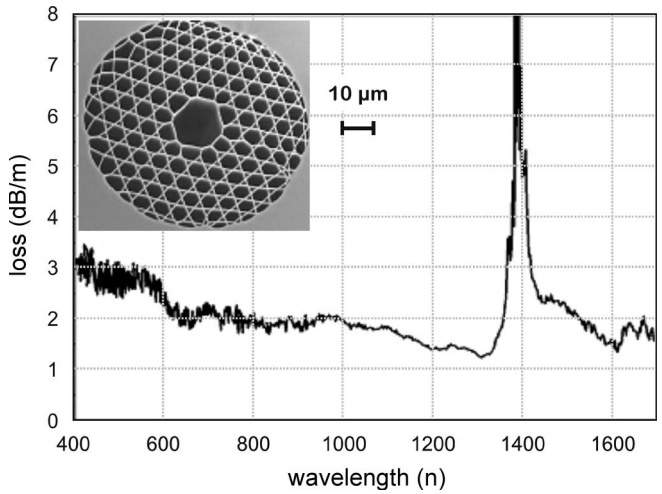

Fig. 13. Measured loss of a hollow-core PCF with a Kagomé cladding lattice (scanning electron micrograph of structure in the inset). This type of photonic crystal provides a low density of states, i.e., an incomplete band gap. The peak at around 1390 nm is due to absorption by an overtone of the OH resonance.

large glass–air index difference means that even slight accidental distortions in the structure yield a degree of birefringence. Therefore, if the core is deliberately distorted so as to become twofold symmetric, extremely high values of birefringence can be achieved. For example, by introducing capillaries with different wall thicknesses above and below a solid glass core [Figs. 8(h) and 14(a)], values of birefringence some ten times larger than in conventional fibers can be obtained [20]. Hollow-core PCF with moderate levels of birefringence ($\sim 10^{-4}$) can be realized either by forming an elliptical core or by adjusting the structural design of the core surround [66], [67].

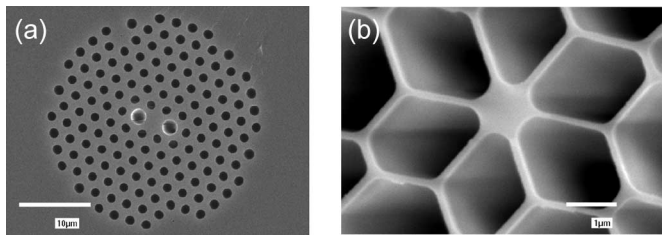

Fig. 14. (a) Scanning electron micrographs of two different PCFs. (a) Birefringent PCF. (b) PCF with very small core (diameter 800 nm) and zero GVD wavelength 560 nm.

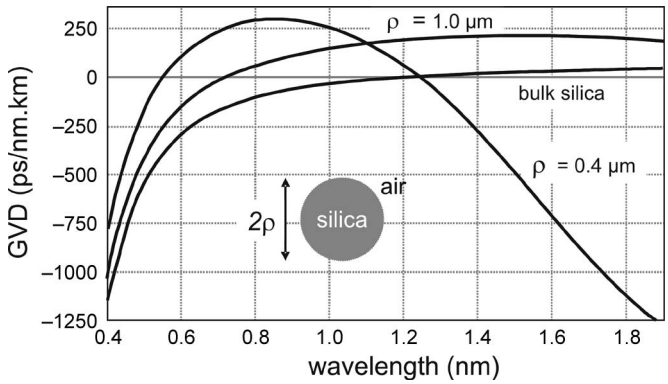

Fig. 15. Calculated GVD of two circular strands of silica glass, radii 0.4 and 1.0 μm, compared with the dispersion of bulk glass. The narrower strand has two dispersion zeros within the transparency window of silica.

Experiments show that the birefringence in PCFs is some 100 times less sensitive to temperature variations than in conventional fibers, which is important in many applications [68]. This is because traditional "polarization-maintaining" fibers (bow-tie, elliptical core, or Panda) contain at least two different glasses, each with a different thermal expansion coefficient. In such structures, the resulting temperature-dependent stresses make the birefringence a strong function of temperature.

E. GVD

GVD, which causes different frequencies of light to travel at different group velocities, is a factor crucial in the design of telecommunications systems and in all kinds of nonlinear optical experiments. PCF offers greatly enhanced control of the magnitude and sign of the GVD as a function of wavelength. In many ways, this represents an even greater opportunity than a mere enhancement of the effective nonlinear coefficient.

1) Solid Core: As the optical frequency increases, the GVD in SMF changes sign from anomalous ($D > 0$) to normal ($D < 0$) at $\sim$1.3 μm. In solid-core PCF, as the holes get larger, the core becomes more and more isolated, until it resembles an isolated strand of silica glass (Fig. 15). If the whole structure is made very small (core diameters less than 1 μm have been made), the zero-dispersion point of the fundamental guided mode can be shifted to wavelengths in the visible [17], [18]. For example, the PCF in Fig. 14(b) has zero dispersion at 560 nm.

By careful design, the wavelength dependence of the GVD can also be reduced in PCFs at much lower air-filling fractions. Fig. 16 shows the flattened GVD profiles of three PCFs with

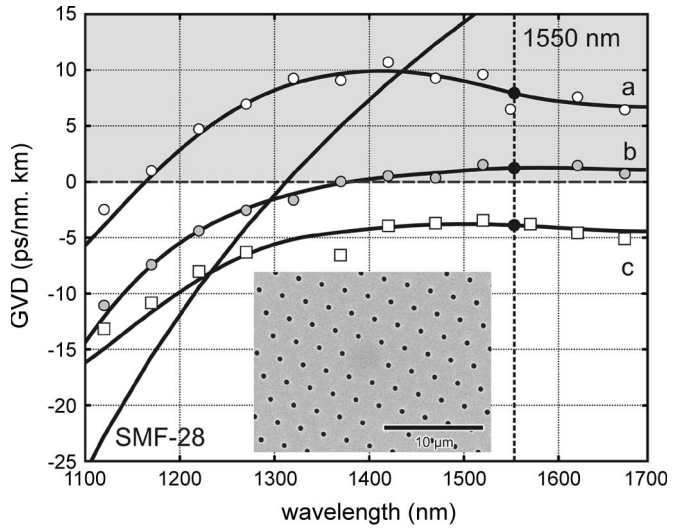

Fig. 16. GVD profiles, against wavelength, for three different PCFs designed to have low-level ultraflattened GVD [69], [70]. The curve for Corning SMF-28 is included for comparison.

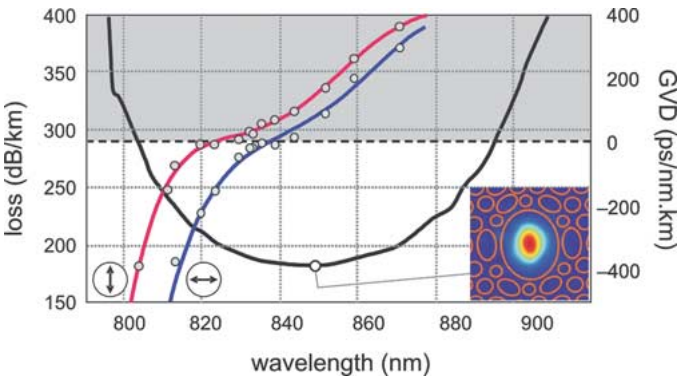

Fig. 17. Measured attenuation and GVD spectra for a hollow-core PCF designed for 850 nm transmission [71]. The core is slightly elliptical, so the dispersion in each eigenstate of polarization is different. The inset shows the measured near-field distribution at 848 nm wavelength (the positions of the air-glass boundaries are marked with orange lines).

cores several micrometers in diameter [69], [70]. These fibers operate in the regime where SMF is multimoded. Although the fundamental modes in both SMF and PCF have similar dispersion profiles, the presence of higher order modes (not guided in the PCF, which is ESM) makes the use of SMF impractical.

A further degree of freedom in GVD design may be gained by working with multicomponent glasses such as Schott SF6, where the intrinsic zero-dispersion point occurs at $\sim$1.8 μm [28]. In a highly nonlinear small-core PCF, this shifts the whole dispersion landscape to longer wavelengths than in a silica-based PCF with the same core size and geometry.

2) Hollow Core: Hollow-core fiber behaves in many respects rather like a circular-cylindrical hollow metal waveguide, which has anomalous dispersion (the group velocity increases as the frequency rises). The main difference, however, is that the dispersion changes sign at the high-frequency edge due to the approach of the photonic band edge and the weakening of the confinement (Fig. 17) [71].

F. Attenuation Mechanisms

An advantage common to all fibers is the very large extension ratio from preform to fiber, which has the effect of smoothing out imperfections, resulting in a transverse structure that is extremely invariant with distance along the fiber. This is the chief reason for the ultralow attenuation displayed by fibers compared to other waveguide structures. In PCFs, the losses are governed by two main parameters, namely the fraction of light in glass and the roughness at the glass–air interfaces. The light-in-glass fraction can be controlled by judicious design and ranges from close to 100% in solid-core fibers to less than 1% in the best hollow-core fibers.

1) Absorption and Scattering: The best loss in solid-core PCF, which was reported by a group in Japan, stands at 0.28 dB/km at 1550 nm, with a Rayleigh-scattering coefficient of 0.85 $\mathrm{dB}\cdot\mathrm{km}^{-1}\cdot\mu\mathrm{m}^{-4}$. One hundred kilometers of this fiber was used in the first PCF-based penalty-free dispersion-managed soliton transmission system at 10 Gb/s [72]. The slightly higher attenuation compared to SMF is due to roughness at the glass–air interfaces [58].

It is hollow-core PCF, however, that has the greatest potential for extremely low loss, since light travels predominantly in empty (or gas-filled) space. Although the best reported attenuation in hollow-core PCF stands at 1.2 dB/km [55], values below 0.2 dB/km or even lower seem feasible with further development of the technology. The prospect of improving on conventional fiber while at the same time greatly reducing the nonlinearities associated with a solid glass core is intriguing. By using IR glasses, transmission can be extended into the IR [73], and a recent work shows that silica hollow-core PCF can even be used with acceptable levels of loss in the mid-IR [74] due to the very low overlap between the optical field and the glass.

In the latest hollow-core silica PCF, with loss levels approaching 1 dB/km at 1550 nm, very small effects can contribute significantly to the attenuation floor. The ultimate loss limit in such fibers is determined by surface roughness caused by thermally-driven capillary waves, which are present at all length scales. These interface ripples freeze in when the fiber cools, introducing high scattering losses for modes that are concentrated at the interfaces such as surface modes guided on the edge of the core. The pure core mode does not itself "feel" the ripples very strongly, except at anticrossing wavelengths where it becomes phase-matched to surface modes, causing light to move to the surface and experience enhanced scattering.

The result is a transmission spectrum consisting of windows of high transparency punctuated with bands of high attenuation (Fig. 18). This picture has been confirmed by measurements of the surface roughness in hollow-core PCFs, the angular distribution of the power scattered out of the core, and the wavelength dependence of the minimum loss of fibers drawn to different scales [55]. The thin glass shell surrounding the hollow core can be designed to be antiresonant with the core mode, permitting further exclusion of light from the glass [75].

Ignoring material dispersion, the whole transmission landscape shifts linearly in wavelength in proportion to the overall

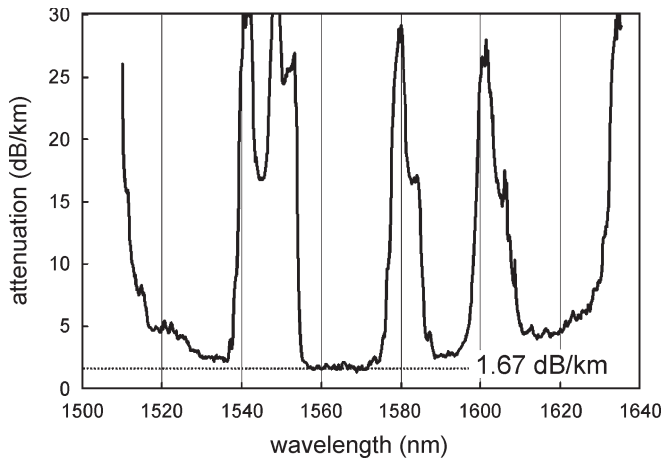

Fig. 18. Attenuation spectrum of a typical ultra-low-loss hollow-core PCF designed for operation in the 1550-nm telecommunications band (see micrograph in Fig. 9).

size of the structure—a consequence of Maxwell's equations. This means that the smallest loss at a given wavelength will be obtained by drawing a fiber to a particular diameter. The optical overlap with the surface roughness scales inversely with the size with the fiber, and the scattering itself may be regarded as being governed by the density of states into which scattering can occur, which, in three dimensions, scales as λ^{-2}. Thus, the wavelength of minimum loss scales as λ^{-3} in contrast to the λ^{-4} dependence of Rayleigh scattering in bulk glass.

2) Bend Loss: Conventional fibers suffer additional loss if bent beyond a certain critical radius $R_{\rm crit}$, which depends on wavelength, core–cladding refractive-index step, and, most notably, the third power of core radius a^3 [38]. For wavelengths longer than a certain value (the "long-wavelength bend edge"), all guidance is effectively lost.

A starting point for understanding bend loss in solid-core ESM-PCF (perhaps the most interesting case) is the long-wavelength limit. ESM behavior occurs when $d/\Lambda < 0.43$, which sets the highest air-filling fraction at 16.8% and yields an area-averaged cladding refractive index of 1.388 (silica index of 1.444)—valid in the limit $k \to 0$. This index step is some ten times higher than in Corning SMF-28, making ESM-PCF relatively much less susceptible to bend loss at long wavelengths. For a step-index fiber with a Ge-doped core, 40 mol% of GeO_2 would be needed to reach the same index step (assuming 0.0014 index change per mol% GeO_2 [4]). The result is that the long-wavelength bend edge in ESM-PCF is in the IR beyond the transparency window of silica glass, even when the core radius is large [76].

ESM-PCF also exhibits a short-wavelength bend edge caused by bend-induced coupling from the fundamental to higher order modes, which, of course, leak out of the core [15]. The critical bend radius for this loss varies as

$$R_{\rm c} \sim \Lambda^3/\lambda^2 \tag{10}$$

compared to $R_{\rm c} \sim \lambda$ for SMF. The reciprocal dependence on λ^2 makes it inevitable for a short-wavelength bend edge to appear in ESM-PCF. Following [76] in taking the prefactor in (10) as unity, $R_{\rm c}$ can be plotted against wavelength for different

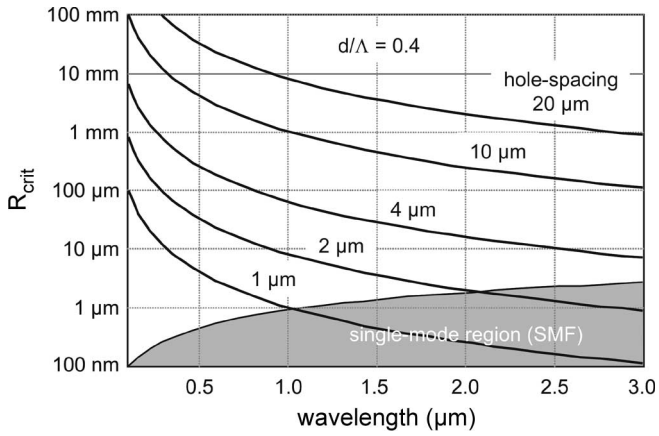

Fig. 19. Short-wavelength critical bend radii for ESM-PCF with $d/\Lambda = 0.4$ plotted against vacuum wavelength for different values of hole spacing (approximately equal to the core radius). As the wavelength increases at constant core size, a step-index fiber with the same core–cladding index difference as the PCF in the long-wavelength limit [using (5)] becomes single mode when the curves enter the shaded region. The step-index fiber is multimode over wide parameter ranges where ESM-PCF has negligible short-wavelength bend loss.

values of core radius (≈interhole spacing). This is illustrated in Fig. 19. A step-index fiber, with the same core–cladding index step as ESM-PCF in the long-wavelength limit, is multimode over wide parameter ranges where ESM-PCF has negligible bend loss.

In contrast, hollow-core PCF is experimentally very insensitive to bend loss—in many cases, no appreciable drop in transmission is observed until the fiber breaks. This is because the effective depth of "potential well" for the guided light (see Section VI-C), which is given by the distance $\Delta\beta$ between the edges of the PBG, is substantially larger than that in SMF.

3) Confinement Loss: The photonic-crystal cladding in a realistic PCF is, of course, finite in extent. For a guided mode, the Bloch waves in the cladding are evanescent, just like the evanescent plane waves in the cladding of a conventional fiber. If the cladding is not thick enough, the evanescent field amplitudes at the cladding/coating boundary can be substantial, causing attenuation. In the solid core case for small values of d/Λ, the resulting loss can be large unless a sufficiently large number of periods is used [69].

Very similar losses are observed in hollow-core fibers, where the "strength" of the PBG (closely related to its width in β) determines how many periods are needed to reduce confinement loss to acceptable levels. Numerical modeling is useful for giving an indication of how many periods are needed to reach a required loss level. The cladding field intensity in the ultra-low-loss PCF reported in [55] falls by ∼9 dB per period, reaching −63 dB at the edge of the photonic-crystal region.

G. Kerr Nonlinearities

The ability to enhance or reduce the effective Kerr nonlinearity and, at the same time, control the magnitude and wavelength dependence of the GVD makes PCF a versatile vehicle for studies of effects such as four-wave mixing, self-phase modulation, modulation instability, soliton formation, and stimulated Raman scattering. To take account of the differing proportions

of light in glass and air, it is necessary to redefine the γ coefficient [77] as follows:

$$\gamma = k \sum_i n_2^i / A_{\text{eff}}^i = k\, n_2^{\text{eff}} / A_{\text{core}}. \tag{11}$$

In (11), n_2^i is the nonlinear refractive index of material i (i.e., 2.9×10^{-23} m$^2 \cdot$ W^{-1} for air, 2.5×10^{-20} m$^2 \cdot$ W^{-1} for silica, and an order of magnitude or more higher for multicomponent glasses), A_{eff}^i is defined as the effective area for the light in material i, and n_2^{eff} is the effective nonlinear index for the fiber (core area A_{core}).

The highest nonlinearity available in conventional step-index fibers is $\gamma = 20$ W$^{-1} \cdot$ km^{-1} at 1550 nm [78]. By comparison, a solid-core PCF similar to the one in Fig. 14(b) but with a core diameter of 1 μm has a nonlinearity of $\gamma = 240$ W$^{-1} \cdot$ km^{-1} at 850 nm, and values as high as $\gamma = 550$ W$^{-1} \cdot$ km^{-1} at 1550 nm have been measured for PCFs made from multicomponent glasses [79].

In complete contrast, hollow-core PCF has extremely low levels of nonlinearity due to the small overlap between the glass and the light. In a recent example, a fiber was reported with an effective nonlinear refractive index of $n_2^{\text{eff}} = 8.6 \times 10^{-23}$ m$^2 \cdot$ W^{-1} (roughly 300 times smaller than in silica glass), and a nonlinear coefficient $\gamma = 0.023$W$^{-1} \cdot$ km^{-1} (some $10^4\times$ smaller than in a typical highly nonlinear solid-core PCF) [80].

Although the level of nonlinearity is clearly important, the actual nonlinear effects that appear in a particular case are also strongly dependent on the magnitude, sign, and wavelength dependence of the GVD (see Section VII-D) as well as on the characteristics of the pump laser [81].

VII. Applications

The diversity of new or improved features beyond conventional fibers means that PCFs are finding an increasing number of applications in ever-widening areas of science and technology.

A. High-Power and -Energy Transmission

ESM-PCF's ability to remain single mode at all wavelengths where it guides, and for all scales of structure, suggests that it should have superior power-handling properties—the core area can be increased without the penalty of introducing higher order guided modes [16]. The ability to transmit much higher power in a single mode has a major impact in the field of laser machining and high-power fiber lasers and amplifiers. The key issue is bend loss, and as we have seen, it turns out that PCF offers a wider bandwidth of useful single-mode guidance than high-Δ SMF, because it can operate in the multimode regime of SMF while remaining single mode (Section VI-B1). This also allows the long-wavelength bend edge to be moved to longer wavelengths.

Hollow-core PCF is also an excellent candidate for transmitting high continuous-wave power as well as ultrashort pulses with very high peak powers. Solitons have been reported at 1550 nm with durations of 100 fs and peak powers of 2 MW [82] and at 800 nm using a Ti:sapphire laser [80]. The soliton energy is, of course, determined by the effective value of γ and the magnitude of the anomalous GVD. As mentioned in Section VI-E2, the GVD changes sign across the band gap, permitting choice of normal or anomalous dispersion, depending upon the application [71]. Further studies explore the ultimate power-handling capacity of hollow-core PCF [59], [83], [84].

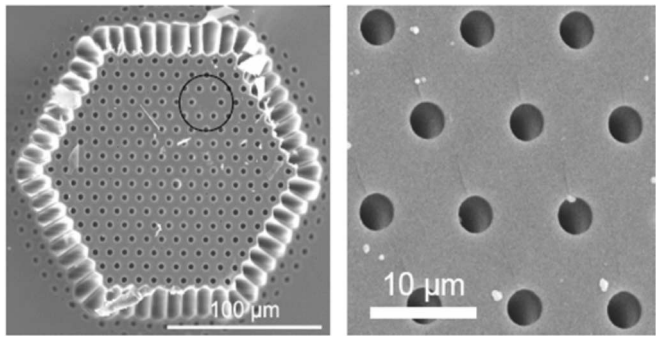

Fig. 20. Scanning electron micrograph of an air-clad fiber (Yb-doped core circled). The structural parameters are listed as follows: hole-spacing 9.6 μm; $d/\Lambda = 0.4$; core diameter 15.2 μm; 54 webs of width 350 nm; inner cladding diameter 143 μm across flats; 164 μm across corners [87].

B. Fiber Lasers and Amplifiers

PCF lasers can be straightforwardly produced by incorporating a rare-earth-doped cane in the preform stack. Many different designs can be realized such as cores with ultralarge mode areas for high power and structures with multiple lasing cores [85]. Cladding-pumping geometries for ultrahigh power can be fashioned by incorporating a second core (much larger and multimode) around a large off-center ESM lasing core. Using microstructuring techniques, this "inner cladding waveguide" can be suspended by connecting it to an outer glass tube with very thin webs of glass (see Fig. 20) [86]. This results in a very large effective index step and, thus, a high numerical aperture (> 0.9), making it easy to launch and guide light from high-power diode-bar pump lasers, which typically have poor beam quality. The multimode pump light is efficiently absorbed by the lasing core, and high-power single-mode operation can be achieved [87]–[89]. In one report, a microchip-laser-seeded Yb-doped PCF amplifier generated diffraction-limited 0.45-ns-duration pulses with a peak power of 1.1 MW and a peak spectral brightness greater than 10 kW$/$(cm$^2 \cdot$ sr $\cdot$ Hz) [90].

Hollow-core PCF, with its superior power handling and designable GVD, is ideal as the last compression stage in chirped-pulse amplification schemes. This permits operation at power densities that would destroy conventional glass-core fibers [91], [92].

C. Intrafiber Devices—Cutting and Joining

As PCF becomes more widely used, there is an increasing need for effective cleaves, low-loss splices, multiport couplers, intrafiber devices, and mode-area transformers. The air holes provide an opportunity not available in standard fibers: the creation of dramatic morphological changes by altering the hole

size by collapse (under surface tension) or inflation (under internal overpressure) when heating to the softening temperature of the glass. Thus, not only can the fiber be stretched locally to reduce its cross-sectional area, but also, the microstructure can itself be radically altered.

1) Cleaving and Splicing: PCFs cleave cleanly using standard tools, showing slight end face distortion only when the core crystal is extremely small (interhole spacing $\sim$1 μm) and the air-filling fraction is very high ($>$ 50%). Solid glass end caps can be formed by collapsing the holes (or filling them with sol–gel glass) at the fiber end to form a coreless structure through which light can be launched into the fiber. A solid-core PCF can be fusion spliced successfully both to itself and to step-index fiber using resistive heating elements (electric arcs do not allow sufficient control). The two fiber ends are placed in intimate contact and heated to softening point. With careful control, they fuse together without distortion. Provided the mode areas are well matched, splice losses of $<$ 0.2 dB can normally be achieved, except when the core is extremely small (i.e., less than $\sim$1.5 μm). Fusion splicing of hollow-core fibers is feasible when there is a thick solid glass outer sheath [e.g., as depicted in Fig. 9(a)], although very low splice losses can be obtained simply by placing identical fibers end-to-end and clamping them (the index-matching "fluid" for hollow-core PCF is vacuum).

The ability to hermetically splice a gas-filled hollow-core PCF to SMF has made it possible to produce in-line gas cells for stimulated Raman scattering in hydrogen and frequency measurement and stabilization (using acetylene). These developments may lead for the first time to practical miniature gas–laser devices that could even be coiled up inside a credit card [93].

2) Mode Transformers: In many applications, it is important to be able to change the mode area without losing light. This is done traditionally using miniature bulk optics—tiny lenses precisely designed to match to a desired numerical aperture and spot size. In PCFs, an equivalent effect can be obtained by scanning a heat source (flame or carbon dioxide laser) along the fiber. This causes the holes to collapse, with the degree of collapse depending on the dwell time of the heat. Drawing the two fiber ends apart at the same time provides additional control. Graded transitions can fairly easily be made—mode diameter reductions as high as 5 : 1 have been realized with low loss.

Ferrule methods have been developed for making low-loss interfaces between conventional SMFs and PCFs [94]. Adapted from the fabrication of PCF preforms from stacked tubes and rods, these techniques avoid splicing and are versatile enough to interface to virtually any type of index-guiding silica PCF (Fig. 21). They are effective for coupling light into and out of all of the individual cores of a multicore fiber without input or output crosstalk. The technique also creates another opportunity—the use of taper transitions to couple light between a multimode fiber and several SMFs. When the number of SMFs matches the number of spatial modes in the multimode fiber, the transition can have low loss in both directions. This means that the high performance of SMF devices can be reached in multimode systems, for example, a multimode fiber

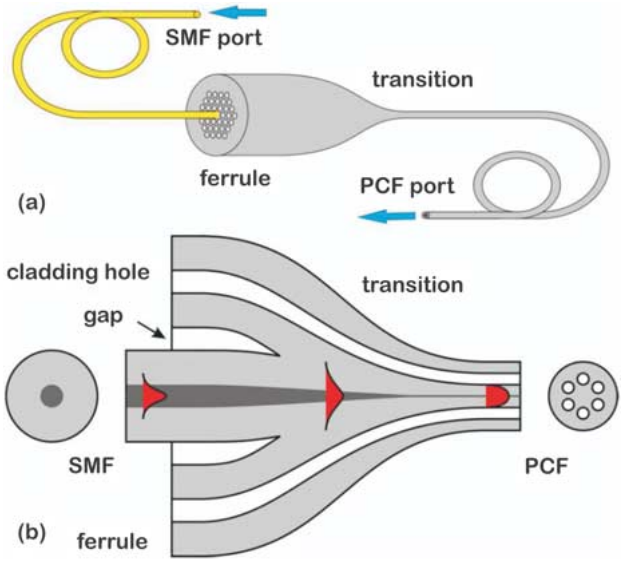

Fig. 21. Schematic (not to scale) of the ferrule tapering technique for creating low-loss interfaces between standard step-index fiber and solid-core PCF. (a) Finished device. (b) Detail of the transition (after [94]).

filter with the transmission spectrum of an SMF Bragg grating [95], which is a device that has applications in earth-based astronomy, where the high throughput of a multimode fiber can be retained while unwanted atmospheric emission lines are filtered out.

A further degree of freedom may be gained by pressurizing the holes during the taper process [96]. The resulting hole inflation permits radical changes in the guidance characteristics. It is possible, for example, to transform a PCF, with a relatively large core and small air-filling fraction, into a PCF with a very small core and a large air-filling fraction, the transitions having very low loss [97].

3) In-Fiber Devices: Precise use of heat and pressure induces large changes in the optical characteristics of PCFs, giving rise to a whole family of new intrafiber components. Microcouplers can be made in a PCF with two optically isolated cores by collapsing the holes to allow the mode fields to expand and interact with each other, creating local coupling [98]. Long-period gratings, which scatter the core light into cladding modes within certain wavelength bands, can be made by periodic modulation of hole size [99]. By rocking a birefringent PCF to and fro while scanning a carbon dioxide laser along it, so-called "rocking filters" can be made, which transfer power from one polarization state to the other within a narrow band of wavelengths [100]. All these components have one great advantage over equivalent devices made in conventional fiber: Because they are formed by permanent changes in morphology, they are highly stable with temperature and over time.

Heating and stretching PCF can result in quite remarkable changes in the scale of the micro/nanostructures without significant distortion. Recently, a solid-core PCF was reduced five times in linear scale, resulting in a core diameter of 500 nm (Fig. 22). This permitted the formation of a PCF with a zero-dispersion wavelength that matched the 532-nm emission wavelength of a frequency-doubled Nd:YAG laser [101] (this is important for SC generation—see Section IV-A). A further

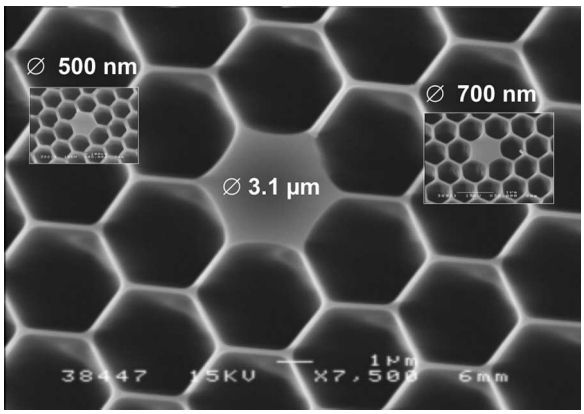

Fig. 22. Scanning electron micrographs (depicted to the same scale) of the fiber cross sections produced by tapering a solid-core PCF. The structures are very well preserved, even down to core diameters of 500 nm [101].

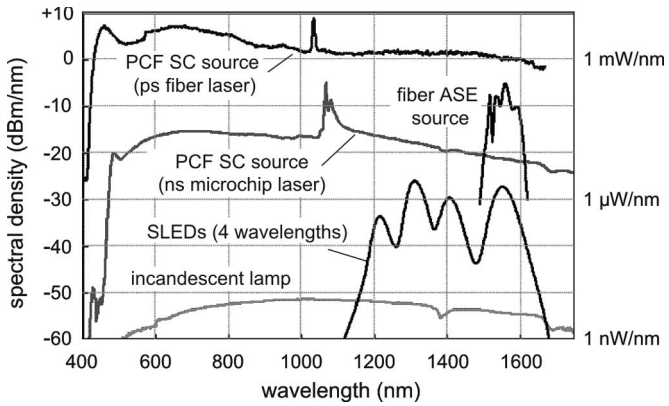

Fig. 23. Comparison of the brightness of various broadband light sources (SLED—superluminescent light-emitting diode; ASE—amplified spontaneous emission; SC—supercontinuum). The microchip laser SC spectrum was obtained by pumping at 1064 nm with 600-ps pulses (updated version of a plot by H. Sabert).

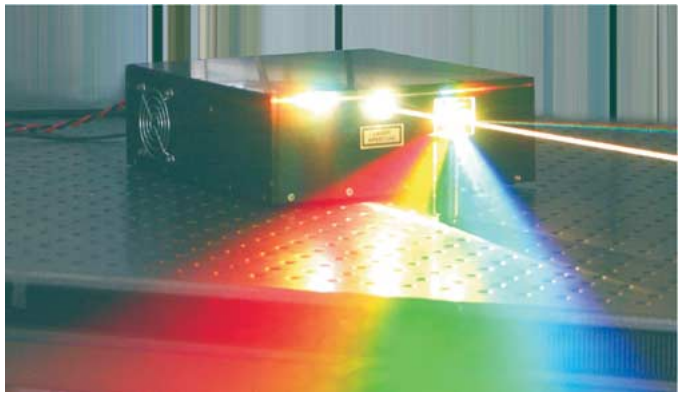

Fig. 24. SC light generated in ESM-PCF from picosecond fiber laser (courtesy of Fianium Ltd.). Total SC power is 6.5 W for a 10-W pump power (5-ps pulses). Repetition rate is 50 MHz, and the average spectral power density in the range 450–800 nm is a remarkable ∼4.5 mW/nm (see also Fig. 23).

compelling advantage of the tapering approach is that it neatly sidesteps the difficulty of launching light into submicrometer-sized cores; light is launched into the entry port (in this case with a core diameter of 2.5 μm) and adiabatically evolves, with negligible loss, into the mode of the 500-nm core.

D. Kerr-Related Nonlinear Effects

The nonlinear characteristics are determined by the relative values of the nonlinear length $L_{\rm nl} = 1/(\gamma P_0)$, where P_0 is the peak power, the dispersion length $L_{\rm D} = \tau^2/|\beta_2|$, where τ is the pulse duration and the effective fiber length $L_{\rm eff} = (1 - \exp(-\alpha L))/\alpha$, where α (in units per meter) is the power attenuation coefficient [102]. For a solid-core PCF with $\gamma \sim 240\ {\rm W}^{-1} \cdot {\rm km}^{-1}$, a peak power of 10 kW yields $L_{\rm nl} < 0.5$ mm. For typical values of loss (usually between 1 and 100 dB/km), $L_{\rm eff} \gg L_{\rm nl}$, and the nonlinearity dominates. For dispersion values in the range $-300 < \beta_2 < 300\ {\rm ps}^2/{\rm km}$ and pulse durations $\tau = 200$ fs, $L_{\rm D} > 0.1$ m. Since both of these lengths are much longer than the nonlinear length, it is easy to observe strong nonlinear effects.

1) SC Generation: One of the most successful applications of nonlinear PCF is to SC generation from picosecond and femtosecond laser pulses. When high-power pulses travel through a material, their frequency spectrum can be broadened by a range of interconnected nonlinear effects [103]. In bulk materials, the preferred pump laser is a regeneratively amplified Ti:sapphire system producing high-energy (in millijoules) femtosecond pulses at 800 nm wavelength and kilohertz repetition rate. SCs have also previously been generated in SMF by pumping at 1064 or 1330 nm [104], with the spectrum broadening out to longer wavelengths mainly due to stimulated Raman scattering (SRS). Then, in 2000, it was observed that highly nonlinear PCFs, which are designed with zero GVD close to 800 nm, massively broaden the spectrum of low-energy (a few nanojoules) unamplified Ti:sapphire pulses launched into just a few centimeters of fiber [22], [105], [106]. Removing the need for a power amplifier, the hugely increased (∼100 MHz) repetition rate as well as the spatial and temporal coherence of the light emerging from the core makes this source unique. The broadening extends to both higher and lower frequencies because four-wave mixing operates more efficiently than SRS when the dispersion profile is appropriately designed. This SC source has applications in optical coherence tomography [107], [108], frequency metrology [109], [110], and all kinds of spectroscopy. It is particularly useful as a bright low-coherence source in measurements of group delay dispersion based on a Mach–Zehnder interferometer.

A comparison of the bandwidth and spectrum available from different broadband light sources is shown in Fig. 23; the advantages of PCF-based SC sources are evident. SCs have been generated in different PCFs at 532 [101], 647 [111], 1064 [112], and 1550 nm [28]. Using inexpensive microchip lasers at 1064 or 532 nm with an appropriately designed PCF, compact SC sources are now available with important applications across many areas of science (Fig. 24 shows a picosecond fiber-laser-based system in operation). The use of multicomponent glasses such as Schott SF6 or tellurite glass allows the balance of nonlinearity and dispersion to be adjusted as well as offering extended transparency into the IR [113].

2) Parametric Amplifiers and Oscillators: In step-index fibers, the performance of optical parametric oscillators and amplifiers is severely constrained owing to the limited scope

for GVD engineering. In PCFs, these constraints are lifted, permitting flattening of the dispersion profile and control of higher order dispersion terms. The wide range of experimentally available GVD profiles has, for example, allowed studies of ultrashort pulse propagation in the 1550-nm wavelength band with flattened dispersion [69], [70]. The effects of higher order dispersion in such PCFs are subtle [114], [115]. Parametric devices have been designed for pumping at 647, 1064, and 1550 nm, the small effective mode areas offering high gain for a given pump intensity, and PCF-based oscillators synchronously pumped by femtosecond and picosecond pump pulses have been demonstrated at relatively low power levels [116]–[119].

3) Correlated Photon Pairs: The use of self-phase modulation to generate bright sources of correlated photon pairs is unsuccessful in step-index fibers due to high Raman-related noise. This is because for $\beta_2 < 0$ and $\beta_n = 0,\ n > 2$, the modulational instability sidebands are situated very close to the pump frequency within the Raman gain band of the glass. By flattening the GVD profile and making β_2 small, however, higher order GVD terms become important, and gain bands can appear in the normal dispersion regime for $\beta_2 > 0$ and $\beta_4 < 0$ [70]. The relevant expression for the sideband gain (in units per meter), including β_4 and β_6, is

$$\text{gain} = \text{Im}\left[\sqrt{Q(Q+2\gamma P)}\right]$$
$$Q = \beta_2\Omega^2/2 + \beta_4\Omega^4/24 + \beta_6\Omega^6/720 \qquad (12)$$

where γ is the nonlinear coefficient (11), P is the pump power, and Ω is the angular frequency offset from the pump frequency. This expression may be used to show that the sidebands can be widely spaced from the pump frequency, their position and width being controllable by engineering the even-order higher order dispersion terms. It is straightforward to arrange that these sidebands lie well beyond the Raman gain band, reducing the Raman noise and allowing PCF to be used as a compact bright tunable single-mode source of photon pairs with wide applications in quantum communications [120], [121]. In a recent example, a PCF with zero dispersion at 715 nm was pumped by a Ti:sapphire laser at 708 nm (normal dispersion) [122]. Under these conditions, phase matching is satisfied by signal and idler waves at 587 and 897 nm, and 10 million photon pairs per second were generated and delivered via SMF to Si avalanche detectors, producing $\sim 3.2 \times 10^5$ coincidences per second for a pump power of 0.5 mW. These results point the way to practical and efficient sources of entangled photon pairs that can be used as building blocks in future multiphoton interference experiments.

4) Soliton Self-Frequency Shift Cancellation: The ability to create PCFs with negative dispersion slope at the zero-dispersion wavelength (in SMFs, the slope is positive, i.e., the dispersion becomes more anomalous as the wavelength increases) has made it possible to observe Čerenkov-like effects in which solitons (which form on the anomalous side of the dispersion zero) shed power into dispersive radiation at longer wavelengths on the normal side of the dispersion zero. This occurs because higher order dispersion causes the edges of the soliton spectrum to phase-match to linear waves. The result is the stabilization of the soliton self-frequency shift at the cost of gradual loss of soliton energy [123]. The behavior of solitons in the presence of wavelength-dependent dispersion is the subject of many recent studies, for example, [124].

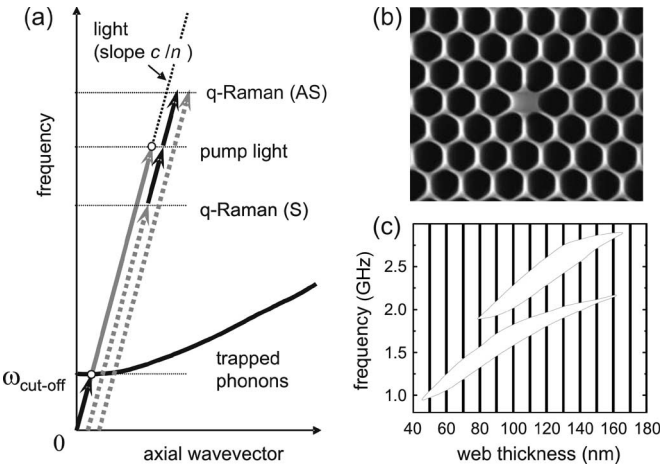

Fig. 25. (a) Illustration of how a trapped acoustic phonon can phase-match to light at the acoustic cutoff frequency. The result is a quasi-Raman scattering process that is automatically phase-matched. (b) Example of PCF used in studies of Brillouin scattering (core diameter 1.1 μm). (c) Frequencies of full phononic band gaps (in-plane propagation and pure in-plane motion) in the cladding of the PCF in (b) (after [130]).

E. Brillouin Scattering

The periodic micro/nanostructuring in ultrasmall core glass–air PCFs strongly alters the acoustic properties compared to conventional SMFs [125]–[128]. Sound can be guided in the core both as leaky and as tightly confined acoustic modes. In addition, the complex geometry and "hard" boundaries cause coupling between all three displacement components (radial, azimuthal, and axial), with the result that each acoustic mode has elements of both shear (S) or longitudinal (L) strain. This complex acoustic behavior strongly alters the characteristics of forward and backward Brillouin scattering.

1) Backward Scattering: When a solid-core silica–air PCF has a core diameter of around 70% of the vacuum wavelength of the launched laser light [Fig. 25(b)] and the air-filling fraction in the cladding is very high, the spontaneous Brillouin signal displays multiple bands with Stokes frequency shifts in the 10-GHz range. These peaks are caused by discrete guided acoustic modes, each with different proportions of longitudinal and shear strain strongly localized to the core [129]. At the same time, the threshold power for stimulated Brillouin scattering increases fivefold—a rather unexpected result, since conventionally, one would assume that higher intensities yield lower nonlinear threshold powers. This occurs because the effective overlap between the tightly confined acoustic modes and the optical mode is actually smaller than in a conventional fiber core; the sound field contains a large proportion of shear strain, which does not contribute significantly to changes in refractive index. This is of direct practical relevance to parametric amplifiers, which can be pumped five times harder before stimulated Brillouin scattering appears.

2) Forward Scattering: The very high air-filling fraction in the small-core PCF also permits sound at frequencies of a few gigahertz to be trapped purely in the transverse plane by phononic band gap effects (Fig. 25). The ability to confine acoustic energy at zero axial wavevector $\beta_{\text{ac}} = 0$ means that the ratio of frequency ω_{ac} to wavevector β_{ac} becomes arbitrarily large as $\beta_{\text{ac}} \to 0$ and, thus, can easily match the value for the light guided in the fiber, i.e., c/n. This permits phase-matched interactions between the acoustic mode and two spatially identical optical modes of different frequencies [130]. Under these circumstances, the acoustic mode has a well-defined cutoff frequency $\omega_{\text{cut-off}}$ above which its dispersion curve—plotted on an (ω, β) diagram—is flat, which is similar to the dispersion curve for optical phonons in diatomic lattices. The result is a scattering process that is Raman like (i.e., the participating phonons are optical phonon like), even though it makes use of acoustic phonons; Brillouin scattering is turned into Raman scattering, power being transferred into an optical mode of the same order, frequency-shifted from the pump frequency by the cutoff frequency. Used in stimulated mode, this effect may permit the generation of combs of frequencies spaced by $\sim$2 GHz at 1550 nm wavelength.

F. Gas-Based Nonlinear Optics

It is 100 years since Lord Rayleigh first explained the relationship between depth of focus and focal spot size. The diffraction of light beams in free space presents an apparently insuperable barrier to achieving efficient nonlinear interactions between laser light and low-density media such as gases. The requirements of high intensity, long interaction length, and good-quality (preferably single mode) transverse beam profiles simply cannot be met. A structure conceptually capable of delivering all these requirements simultaneously would be a perfectly guiding hollow-core waveguide supporting a single transverse mode with low attenuation losses. Although, theoretically, this could be realized using a perfect metal, the attenuation in real metals at optical frequencies is much too high, especially when the bore is small enough to yield single-mode operation. A number of conventional approaches have been used to circumvent this problem, including focusing a laser beam into a gas with suitable optics, using a $\sim$100 μm bore fiber capillary to confine the gas and provide some degree of guidance for the light [131], and employing a gas-filled high-finesse Fabry–Pérot cavity to increase the interaction length [132]. None of these approaches comes close, however, to the performance offered by hollow-core PCF [49]. At a bore diameter of 10 μm, for example, a focused free-space laser beam is marginally preferable to a capillary, whereas a hollow-core PCF with a 1.2-dB/km attenuation is 1 million$\times$ more effective. Such huge enhancements are rare, and are leading to dramatic improvements in all sorts of nonlinear laser–gas interactions.

1) Stimulated Raman Scattering: In 2002, stimulated Raman scattering was reported in a hydrogen-filled hollow-core PCF at threshold pulse energies $\sim$100$\times$ lower than previously possible [49]. More recently, the threshold power for rotational Raman scattering in hydrogen was reduced by more than a million times in a single-pass geometry, and near-perfect quantum efficiency was achieved [133]. Such gas cells have been hermetically spliced to standard all-solid glass SMFs [93].

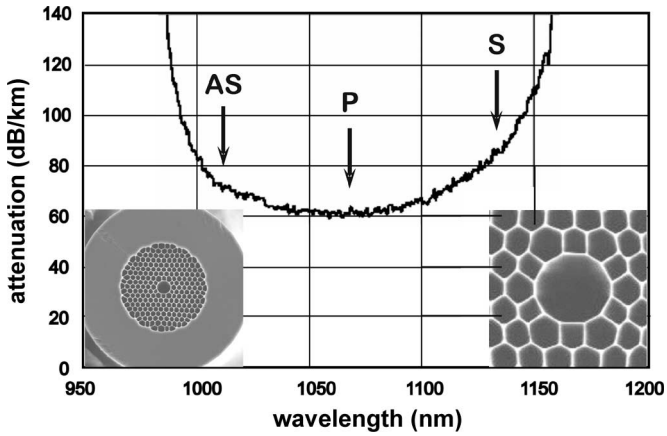

Fig. 26. Attenuation spectrum of a hollow-core PCF designed for low-loss transmission of 1064 nm light. The pump, Stokes, and anti-Stokes Raman frequencies for rotational scattering in hydrogen are marked in. The vibrational Raman band lies well outside the low-loss window.

The limited wavelength ranges of guidance in hollow core are used to advantage here, making it possible to suppress the normally dominant vibrational Raman signal from hydrogen, and enhance the rotational Raman signal, using the PCF in Fig. 26.

2) High Harmonic Generation: Hollow core PCF is likely to have a major impact in other areas of nonlinear optics, such as x-ray generation in noble gases pumped by fs Ti:sapphire laser pulses [135]. The conversion efficiency of this process could be further enhanced by modulating the bore diameter of the core so as to phase-match the light and the x-rays (this was recently demonstrated in simple glass capillaries [136]). In a hollow core PCF this could be implemented for example by heat treatment with carbon dioxide laser light.

3) Electromagnetically Induced Transparency: Hollow-core PCF filled with acetylene vapor at low pressure has recently been used to demonstrate 70% electromagnetically induced transparency (for both Λ-type and V-type interactions) over several lines of the R-branch of the $\nu_1 + \nu_3$ ro-vibrational overtone band [136], [137]. The well-controlled single-mode environment provided by hollow-core PCF makes effects of this kind much easier to control, monitor, and engineer into a practical devices.

G. Telecommunications

There are many potential applications of PCFs or PCF-based devices in telecommunications, although whether these will be adopted remains an open question. One application that seems quite close to being implemented is the use of solid-core PCF or "hole-assisted" SMF for fiber-to-the-home, where the lower bend loss is the attractive additional advantage offered by the holey structure [138]. Other possibilities include dispersion-compensating fiber and hollow-core PCF for long-haul transmission. Additional opportunities exist in producing bright sources of correlated photon pairs for quantum cryptography, parametric amplifiers with improved

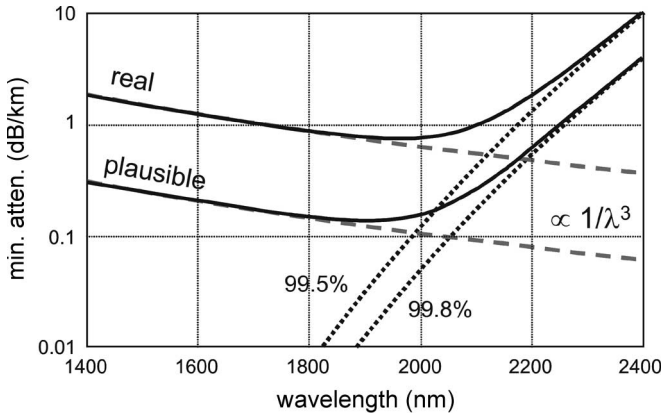

Fig. 27. Realized (real) and plausible minimum attenuation spectra for hollow-core PCF. The scattering floor is proportional to λ^{-3}, with its overall level depending on the amplitude of the surface roughness. Higher air-filling percentages push the IR absorption edge out to longer wavelengths. As a result, the predicted low-loss window sits at 1900 nm, with an attenuation of 0.2 dB/km [55].

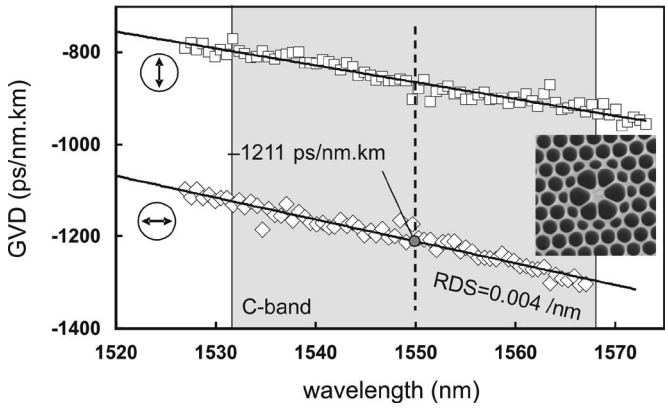

Fig. 28. Performance of a PCF designed to provide slope-matched dispersion compensation for Corning SMF-28 over the C-band.

characteristics, highly nonlinear fiber for all-optical switching and amplification, acetylene-filled hollow-core PCF for frequency stabilization at 1550 nm, and the use of sliced SC spectra as WDM channels. There are also many possibilities for ultrastable in-line devices based on permanent morphological changes in the local holey structure induced by heating, collapse, stretching, or inflation.

1) New Telecommunications Window?: Hollow-core PCF is radically different from solid-core SMF in many ways. This makes it difficult to predict whether it could be successfully used in long-haul telecommunications as a realistic competitor for SMF-28. The much lower Kerr nonlinearities mean that WDM channels can be much more tightly packed without nonlinear crosstalk, and the higher power-handling characteristics mean that more overall power can be transmitted. The effective absence of bend losses is also a significant advantage, particularly for short-haul applications. On the other hand, work still needs to be done to reduce the losses to 0.2 dB/km or lower, and to understand—and control—effects such as polarization mode dispersion, differential group delay, and multipath interference. It is interesting that the low-loss window of a plausible hollow-core PCF is centered at 1900 nm, because light travels predominantly in the hollow regions, completely changing the balance between scattering and IR absorption (Fig. 27) [55].

2) Dispersion Compensation: The large glass–air refractive-index difference makes it possible to design and fabricate PCFs with high levels of GVD. A PCF version of the classical W-profile dispersion compensating fiber was recently reported, offering slope-matched dispersion compensation for SMF-28 fiber at least over the entire C-band (Fig. 28). Dispersion values of -1200 ps/nm $\cdot$ km imply that only 1 km of fiber is needed to compensate for 80 km of SMF-28. The fiber was made deliberately birefringent to allow control of polarization mode dispersion [139].

H. Laser Tweezers in Hollow-Core PCF

A focused light beam produces both a longitudinal (accelerating) and a transverse (trapping) force on dielectric microparticles [140]. For maximum trapping force, the intensity gradient of the light must be as high as possible. This can be achieved by focusing a high-power laser beam with a high numerical aperture lens. The Rayleigh length for such a tightly focused beam is rather short; furthermore, the high intensity will quickly accelerate the particle out of the trapping zone. Stable trapping of a particle in free space requires the longitudinal force to be balanced either by gravity or by a second (or reflected) beam. It has long been recognized that an alternative configuration offering stability would be a nondiffracting or guided beam. To guide a dielectric particle, the beam would have to be trapped in air rather than in glass, which until very recently was not possible. That did not prevent the demonstration of guidance of both solid particles [141] and atoms [142] along lengths of hollow capillary. Of course, use of a capillary prevented the full exploitation of the possibilities of a hollow waveguide; small core sizes are needed for strong transverse confinement, so that capillary losses are very high, even on length scales of a few millimeters. The same is not true in hollow-core PCF, where core diameters of $\sim$10 μm can be realized with losses as low as 50 dB/km. Such a small spot size gives a strong transverse trapping force for a given longitudinal force so that it becomes possible to envisage guiding particles even along tightly coiled fibers at reasonably high speeds. The first steps toward achieving this goal were recently taken [143].

I. Optical Sensors

Sensing is thus far a relatively unexplored area for PCFs, although the opportunities are myriad, spanning many fields including environmental monitoring, biomedical sensing, and structural monitoring [144]. Multicore PCF has been used in bend and shape sensing [51], [145] and Doppler difference velocimetry [146], double-clad PCF in multiphoton fluorescence measurements in medicine [53], and solid-core PCF for hydrostatic pressure sensing [147].

VIII. Final Remarks

In writing this review, I have not been able to cover every topic, nor mention every publication, in a field that is growing by the day. Nevertheless, I hope that my subjective selection

makes clear that, by moving away from constraints of conventional fiber optics, PCFs have created new opportunities in diverse areas of science and technology. Already there is take-up of PCFs in many fields, including compact SC sources, frequency comb systems for frequency metrology, constrained photo- or biochemistry and microfluidics (making use of the hollow channels [148]), biophotonic and biomedical devices, medical imaging, astronomy, particle delivery, high-power fiber lasers, fiber delivery of high-power laser light in manufacturing, and gas-based fiber devices. The next decade should see many of these applications mature into commercial products.

APPENDIX

The analysis in [15] to estimate $n_{\max}$ in a triangular lattice of air holes leads to the following equation:

$$wI_1(a_n w)\left(J_1(bu)Y_0(a_n u) - J_0(a_n u)Y_1(bu)\right) + uI_0(a_n w)\left(J_1(bu)Y_1(a_n u) - J_1(a_n u)Y_1(bu)\right) = 0 \quad (13)$$

where $a_n = d/2\Lambda$, $b = (\sqrt{3}/2\pi)^{1/2}$ (needed to ensure the correct value of $n_{\max}$ in the long-wavelength limit), and $u^2 + w^2 = v^2$. The leading root of (13), which is evaluated for $a_n = 0.2$ and $n_g = 1.444$, yields the polynomial fit (7).

REFERENCES

[1] J. C. Knight, T. A. Birks, P. St.J. Russell, and D. M. Atkin, "Pure silica single-mode fiber with hexagonal photonic crystal cladding," presented at the Conf. Optical Fiber Commun. (OFC), San Jose, CA, Mar. 1996, Postdeadline Paper PD3.

[2] P. St.J. Russell, "Photonic crystal fibers," *Science*, vol. 299, no. 5605, pp. 358–362, Jan. 2003.

[3] [Online]. Available: http://www.corning.com/opticalfiber/

[4] E. M. Dianov and V. M. Mashinsky, "Germania-based core optical fibers," *J. Lightw. Technol.*, vol. 23, no. 11, pp. 3500–3508, Nov. 2005.

[5] P. St.J. Russell, "Designing photonic crystals," in *Electron and Photon Confinement in Semiconductor Nanostructures*. Amsterdam, The Netherlands: IOS, 2003, pp. 79–103.

[6] C. M. Bowden, J. P. Dowling, and H. O. Everitt, "Development and applications of materials exhibiting photonic band gaps: Introduction," *J. Opt. Soc. Amer. B, Opt. Phys.*, vol. 10, no. 2, pp. 280–413, Feb. 1993.

[7] P. St.J. Russell, *NATO Advanced Study Institute on Confined Electrons and Holes*, Jul. 1993, Erice, Italy. private notes, May 1991.

[8] P. V. Kaiser and H. W. Astle, "Low-loss single material fibers made from pure fused silica," *Bell Syst. Tech. J.*, vol. 53, no. 6, pp. 1021–1039, 1974.

[9] L. Li, G. Wylangowski, D. N. Payne, and R. D. Birch, "Broad-band metal glass single-mode fiber polarizers," *Electron. Lett.*, vol. 22, no. 19, pp. 1020–1022, Sep. 1986.

[10] A. Rosenberg, R. J. Tonucci, H.-B. Lin, and A. J. Campillo, "Near-infrared two-dimensional photonic band-gap materials," *Opt. Lett.*, vol. 21, no. 11, pp. 830–832, Jun. 1996.

[11] D. H. Pearson and R. J. Tonucci, "Nanochannel glass replica membranes," *Science*, vol. 270, no. 5233, pp. 68–70, Oct. 1995.

[12] T. A. Birks, P. J. Roberts, P. St.J. Russell, D. M. Atkin, and T. J. Shepherd, "Full 2-D photonic band gaps in silica/air structures," *Electron. Lett.*, vol. 31, no. 22, pp. 1941–1943, 1995.

[13] J. C. Knight, T. A. Birks, P. St.J. Russell, and D. M. Atkin, "All-silica single-mode fiber with photonic crystal cladding," *Opt. Lett.*, vol. 21, no. 19, pp. 1547–1549, Oct. 1996.

[14] ——, "All-silica single-mode fiber with photonic crystal cladding: Errata," *Opt. Lett.*, vol. 22, no. 7, pp. 484–485, Apr. 1997.

[15] T. A. Birks, J. C. Knight, and P. St.J. Russell, "Endlessly single-mode photonic crystal fiber," *Opt. Lett.*, vol. 22, no. 13, pp. 961–963, Jul. 1997.

[16] J. C. Knight, T. A. Birks, R. F. Cregan, P. St.J. Russell, and J.-P. de Sandro, "Large mode area photonic crystal fiber," *Electron. Lett.*, vol. 34, no. 13, pp. 1347–1348, Jun. 1998.

[17] D. Mogilevtsev, T. A. Birks, and P. St.J. Russell, "Group-velocity dispersion in photonic crystal fibers," *Opt. Lett.*, vol. 23, no. 21, pp. 1662–1664, Nov. 1998.

[18] J. C. Knight, J. Arriaga, T. A. Birks, A. Ortigosa-Blanch, W. J. Wadsworth, and P. St.J. Russell, "Anomalous dispersion in photonic crystal fibers," *IEEE Photon. Technol. Lett.*, vol. 12, no. 7, pp. 807–809, Jul. 2000.

[19] R. F. Cregan, B. J. Mangan, J. C. Knight, T. A. Birks, P. St.J. Russell, P. J. Roberts, and D. C. Allan, "Single-mode photonic band gap guidance of light in air," *Science*, vol. 285, no. 5433, pp. 1537–1539, Sep. 1999.

[20] A. Ortigosa-Blanch, J. C. Knight, W. J. Wadsworth, J. Arriaga, B. J. Mangan, T. A. Birks, and P. St.J. Russell, "Highly birefringent photonic crystal fibers," *Opt. Lett.*, vol. 25, no. 18, pp. 1325–1327, Sep. 2000.

[21] B. J. Mangan, J. C. Knight, T. A. Birks, P. St.J. Russell, and A. H. Greenaway, "Experimental study of dual-core photonic crystal fiber," *Electron. Lett.*, vol. 36, no. 16, pp. 1358–1359, Aug. 2000.

[22] J. K. Ranka, R. S. Windeler, and A. J. Stentz, "Visible continuum generation in air–silica microstructure optical fibers with anomalous dispersion at 800 nm," *Opt. Lett.*, vol. 25, no. 1, pp. 25–27, Jan. 2000.

[23] V. N. Melekin and A. B. Manenkov, "Dielectric tube as a low-loss waveguide," *Sov. Phys.—Tech. Phys.*, vol. 13, no. 12, pp. 1698–1699, 1968.

[24] P. Yeh and A. Yariv, "Bragg reflection waveguides," *Opt. Commun.*, vol. 19, no. 3, pp. 427–430, Dec. 1976.

[25] F. Brechet, P. Roy, J. Marcou, and D. Pagnoux, "Single mode propagation in depressed-core-index photonic-bandgap fiber designed for zero-dispersion propagation at short wavelengths," *Electron. Lett.*, vol. 36, no. 6, pp. 514–515, Mar. 2000.

[26] S. G. Johnson, M. Ibanescu, M. Skorobogatiy, O. Weisberg, T. D. Engeness, M. Soljacic, S. A. Jacobs, J. D. Joannopoulos, and Y. Fink, "Low-loss asymptotically single-mode propagation in large-core omniguide fibers," *Opt. Express*, vol. 9, no. 13, pp. 748–779, Dec. 2001.

[27] D. C. Allan, J. A. West, J. C. Fajardo, M. T. Gallagher, K. W. Koch, and N. F. Borrelli, "Photonic crystal fibers: Effective index and bandgap guidance," in *Photonic Crystals and Light Localisation in the 21st Century*, C. M. Soukoulis, Ed. Norwell, MA: Kluwer, 2001, pp. 305–320.

[28] V. V. Ravi Kanth Kumar, A. K. George, W. H. Reeves, J. C. Knight, P. St.J. Russell, F. G. Omenetto, and A. J. Taylor, "Extruded soft glass photonic crystal fiber for ultrabroad supercontinuum generation," *Opt. Express*, vol. 10, no. 25, pp. 1520–1525, Dec. 2002.

[29] K. M. Kiang, K. Frampton, T. M. Monro, R. Moore, J. Tucknott, D. W. Hewak, D. J. Richardson, and H. N. Rutt, "Extruded single-mode non-silica glass holey optical fibers," *Electron. Lett.*, vol. 38, no. 12, pp. 546–547, Jun. 2002.

[30] V. V. Ravi Kanth Kumar, A. K. George, J. C. Knight, and P. St.J. Russell, "Tellurite photonic crystal fiber," *Opt. Express*, vol. 11, no. 20, pp. 2641–2645, Oct. 2003.

[31] R. Bise and D. J. Trevor, "Sol–gel derived microstructured fiber: Fabrication and characterization," presented at the Conf. Optical Fiber Commun. (OFC), Anaheim, CA, Mar. 6–11, 2005.

[32] M. C. J. Large, S. Ponrathnam, A. Argyros, I. Bassett, N. S. Punjari, F. Cox, G. W. Barton, and M. A. van Eijkelenborg, "Microstructured polymer optical fibres: New opportunities and challenges," *Mol. Cryst. Liq. Cryst.*, vol. 446, pp. 219–231, 2006.

[33] D. Mogilevtsev, T. A. Birks, and P. St.J. Russell, "Localised function method for modelling defect modes in 2-D photonic crystals," *J. Lightw. Technol.*, vol. 17, no. 11, pp. 2078–2081, Nov. 1999.

[34] A. Ferrando, J. J. Miret, E. Silvestre, P. Andrés, and M. V. Andrés, "Full-vector analysis of a realistic photonic crystal fiber," *Opt. Lett.*, vol. 24, no. 5, pp. 276–278, Mar. 1999.

[35] P. J. Roberts and T. J. Shepherd, "The guidance properties of multi-core photonic crystal fibers," *J. Opt. A, Pure Appl. Opt.*, vol. 3, no. 6, pp. S133–S140, Nov. 2001.

[36] R. C. McPhedran, L. C. Botten, A. A. Asatryan, N. A. Nicorovici, P. A. Robinson, and C. M. de Sterke, "Calculation of electromagnetic properties of regular and random arrays of metallic and dielectric cylinders," *Phys. Rev. E, Stat. Phys. Plasmas Fluids Relat. Interdiscip. Top.*, vol. 60, no. 6, pp. 7614–7617, Dec. 1999.

[37] T. P. White, B. T. Kuhlmey, R. C. McPhedran, D. Maystre, G. Renversez, C. M. de Sterke, and L. C. Botten, "Multipole method for microstructured optical fibers—1: Formulation," *J. Opt. Soc. Amer. B, Opt. Phys.*, vol. 19, no. 10, pp. 2322–2330, Oct. 2002.

[38] A. W. Snyder and J. D. Love, *Optical Waveguide Theory*. London, U.K.: Chapman & Hall, 1983.

[39] T. A. Birks, D. M. Bird, T. D. Hedley, J. M. Pottage, and P. St.J. Russell, "Scaling laws and vector effects in band gap guiding fibres," *Opt. Express*, vol. 12, no. 1, pp. 69–74, Jan. 2004.

[40] R. D. Meade, A. M. Rappe, K. D. Brommer, J. D. Joannopoulos, and O. L. Alerhand, "Accurate theoretical analysis of photonic band-gap materials," *Phys. Rev. B, Condens. Matter*, vol. 48, no. 11, pp. 8434–8437, Sep. 1993.

[41] J. M. Pottage, D. M. Bird, T. D. Hedley, T. A. Birks, J. C. Knight, P. St.J. Russell, and P. J. Roberts, "Robust photonic band gaps for hollow core guidance in PCF made from high index glass," *Opt. Express*, vol. 11, no. 22, pp. 2854–2861, Nov. 2003.

[42] G. J. Pearce, T. D. Hedley, and D. M. Bird, "Adaptive curvilinear coordinates in a plane-wave solution of Maxwell's equations in photonic crystals," *Phys. Rev. B, Condens. Matter*, vol. 71, no. 19, p. 195108, May 2005.

[43] T. M. Monro, D. J. Richardson, N. G. R. Broderick, and P. J. Bennett, "Holey optical fibers: An efficient modal model," *J. Lightw. Technol.*, vol. 17, no. 6, pp. 1093–1102, Jun. 1999.

[44] C. T. Chan, Q. L. Yu, and K. M. Ho, "Order N spectral method for electromagnetic waves," *Phys. Rev. B, Condens. Matter*, vol. 51, no. 23, pp. 16635–16642, Jun. 1995.

[45] C. Mias, J. P. Webb, and R. L. Ferrari, "Finite element modelling of electromagnetic waves in doubly and triply periodic structures," *Proc. Inst. Electr. Eng.—Optoelectronics*, vol. 146, no. 2, pp. 111–118, Apr. 1999.

[46] A. Hochman and Y. Leviatan, "Analysis of strictly bound modes in photonic crystal fibers by use of a source-model technique," *J. Opt. Soc. Amer. A, Opt. Image Sci.*, vol. 21, no. 6, pp. 1073–1081, Jun. 2004.

[47] J. C. Knight, T. A. Birks, P. St.J. Russell, and J.-P. de Sandro, "Properties of photonic crystal fiber and the effective index model," *J. Opt. Soc. Amer. A, Opt. Image Sci.*, vol. 15, no. 3, pp. 748–752, Mar. 1998.

[48] J. C. Knight, J. Broeng, T. A. Birks, and P. St.J. Russell, "Photonic band gap guidance in optical fibers," *Science*, vol. 282, no. 5393, pp. 1476–1478, Nov. 1998.

[49] F. Benabid, G. Antonopoulos, J. C. Knight, and P. St.J. Russell, "Stimulated Raman scattering in hydrogen-filled hollow-core photonic crystal fiber," *Science*, vol. 298, no. 5592, pp. 399–402, Oct. 2002.

[50] B. J. Mangan, J. Arriaga, T. A. Birks, J. C. Knight, and P. St.J. Russell, "Fundamental-mode cutoff in a photonic crystal fiber with a depressed-index core," *Opt. Lett.*, vol. 26, no. 19, pp. 1469–1471, Oct. 2001.

[51] W. N. MacPherson, M. J. Gander, R. McBride, J. D. C. Jones, P. M. Blanchard, J. G. Burnett, A. H. Greenaway, B. J. Mangan, T. A. Birks, J. C. Knight, and P. St.J. Russell, "Remotely addressed optical fiber curvature sensor using multicore photonic crystal fiber," *Opt. Commun.*, vol. 193, no. 1–6, pp. 97–104, Jun. 2001.

[52] G. Bouwmans, R. M. Percival, W. J. Wadsworth, J. C. Knight, and P. St.J. Russell, "High-power Er:Yb fiber laser with very high numerical aperture pump-cladding waveguide," *Appl. Phys. Lett.*, vol. 83, no. 5, pp. 817–818, Aug. 2003.

[53] M. T. Myaing, J. Y. Ye, T. B. Norris, T. Thomas, J. R. Baker, W. J. Wadsworth, G. Bouwmans, J. C. Knight, and P. St.J. Russell, "Enhanced two-photon biosensing with double-clad photonic crystal fibers," *Opt. Lett.*, vol. 28, no. 14, pp. 1224–1226, Jul. 2003.

[54] N. Y. Joly, T. A. Birks, A. Yulin, J. C. Knight, and P. St.J. Russell, "Linear and nonlinear guidance in an ultralow loss planar glass membrane," *Opt. Lett.*, vol. 30, no. 18, pp. 2469–2471, Sep. 2005.

[55] P. J. Roberts, F. Couny, H. Sabert, B. J. Mangan, D. P. Williams, L. Farr, M. W. Mason, A. Tomlinson, T. A. Birks, J. C. Knight, and P. St.J. Russell, "Ultimate low loss of hollow-core photonic crystal fibers," *Opt. Express*, vol. 13, no. 1, pp. 236–244, 2005.

[56] R. D. Pechstedt and P. St.J. Russell, "Narrow-band in-line fiber filter using surface-guided Bloch modes supported by dielectric multilayer stacks," *J. Lightw. Technol.*, vol. 14, no. 6, pp. 1541–1545, Jun. 1996.

[57] J. West, C. Smith, N. Borrelli, D. Allan, and K. Koch, "Surface modes in air-core photonic band-gap fibers," *Opt. Express*, vol. 12, no. 8, pp. 1485–1496, Apr. 2004.

[58] P. J. Roberts, F. Couny, H. Sabert, B. J. Mangan, T. A. Birks, J. C. Knight, and P. St.J. Russell, "Loss in solid-core photonic crystal fibers due to interface roughness scattering," *Opt. Express*, vol. 13, no. 20, pp. 7779–7793, Oct. 2005.

[59] G. Humbert, J. C. Knight, G. Bouwmans, P. St.J. Russell, D. P. Williams, P. J. Roberts, and B. J. Mangan, "Hollow core photonic crystal fibers for beam delivery," *Opt. Express*, vol. 12, no. 8, pp. 1477–1484, Apr. 2004.

[60] F. Luan, A. K. George, T. D. Hedley, G. J. Pearce, D. M. Bird, J. C. Knight, and P. St.J. Russell, "All-solid photonic bandgap fiber," *Opt. Lett.*, vol. 29, no. 20, pp. 2369–2371, Oct. 2004.

[61] A. Argyros, T. A. Birks, S. G. Leon-Saval, C. M. B. Cordeiro, F. Luan, and P. St.J. Russell, "Photonic bandgap with an index step of one percent," *Opt. Express*, vol. 13, no. 1, pp. 309–314, Jan. 2005.

[62] N. M. Litchinitser, S. C. Dunn, B. Usner, B. J. Eggleton, T. P. White, R. C. McPhedran, and C. M. de Sterke, "Resonances in microstructured optical waveguides," *Opt. Express*, vol. 11, no. 10, pp. 1243–1251, May 2003.

[63] A. Argyros, T. A. Birks, S. G. Leon-Saval, C. M. B. Cordeiro, and P. St.J. Russell, "Guidance properties of low-contrast photonic bandgap fibers," *Opt. Express*, vol. 13, no. 7, pp. 2503–2511, Apr. 2005.

[64] G. Bouwmans, L. Bigot, Y. Quiquempois, F. Lopez, L. Provino, and M. Douay, "Fabrication and characterization of an all-solid 2D photonic bandgap fiber with a low-loss region ($<$ 20 dB/km) around 1550 nm," *Opt. Express*, vol. 13, no. 21, pp. 8452–8459, Oct. 2005.

[65] M. J. Steel, T. P. White, C. N. de Sterke, R. C. McPhedran, and L. C. Botten, "Symmetry and degeneracy in microstructured optical fibers," *Opt. Lett.*, vol. 26, no. 8, pp. 488–490, Apr. 2001.

[66] X. Chen, M. J. Li, N. Venkataraman, M. Gallagher, W. Wood, A. Crowley, J. Carberry, L. Zenteno, and K. Koch, "Highly birefringent hollow-core photonic bandgap fiber," *Opt. Express*, vol. 12, no. 16, pp. 3888–3893, Aug. 2004.

[67] P. J. Roberts, D. P. Williams, H. Sabert, B. J. Mangan, D. M. Bird, T. A. Birks, J. C. Knight, and P. St.J. Russell, "Design of low-loss and highly birefringent hollow-core photonic crystal fiber," *Opt. Express*, vol. 14, no. 16, pp. 7329–7341, 2006.

[68] D. Kim and J. U. Kang, "Sagnac loop interferometer based on polarization maintaining photonic crystal fiber with reduced temperature sensitivity," *Opt. Express*, vol. 12, no. 19, pp. 4490–4495, Sep. 2004.

[69] W. H. Reeves, J. C. Knight, P. St.J. Russell, and P. J. Roberts, "Demonstration of ultra-flattened dispersion in photonic crystal fibers," *Opt. Express*, vol. 10, no. 14, pp. 609–613, Jul. 2002.

[70] W. H. Reeves, D. V. Skryabin, F. Biancalana, J. C. Knight, P. St.J. Russell, F. G. Omenetto, A. Efimov, and A. J. Taylor, "Transformation and control of ultra-short pulses in dispersion-engineered photonic crystal fibers," *Nature*, vol. 424, no. 6948, pp. 511–515, Jul. 2003.

[71] G. Bouwmans, F. Luan, J. C. Knight, P. St.J. Russell, L. Farr, B. J. Mangan, and H. Sabert, "Properties of a hollow-core photonic bandgap fiber at 850 nm wavelength," *Opt. Express*, vol. 11, no. 14, pp. 1613–1620, Jul. 2003.

[72] K. Kurokawa, K. Tajima, K. Tsujikawa, and K. Nakajima, "Penalty-free dispersion-managed soliton transmission over a 100-km low-loss PCF," *J. Lightw. Technol.*, vol. 24, no. 1, pp. 32–37, Jan. 2006.

[73] G. J. Pearce, J. M. Pottage, D. M. Bird, P. J. Roberts, J. C. Knight, and P. St.J. Russell, "Hollow-core PCF for guidance in the mid to far infrared," *Opt. Express*, vol. 13, no. 18, pp. 6937–6946, Sep. 2005.

[74] J. D. Shephard, W. N. MacPherson, R. R. J. Maier, J. D. C. Jones, D. P. Hand, M. Mohebbi, A. K. George, P. J. Roberts, and J. C. Knight, "Single-mode mid-IR guidance in a hollow-core photonic crystal fiber," *Opt. Express*, vol. 13, no. 18, pp. 7139–7144, Sep. 2005.

[75] P. J. Roberts, D. P. Williams, B. J. Mangan, H. Sabert, F. Couny, W. J. Wadsworth, T. A. Birks, J. C. Knight, and P. St.J. Russell, "Realizing low loss air core photonic crystal fibers by exploiting an antiresonant core surround," *Opt. Express*, vol. 13, no. 20, pp. 8277–8285, Oct. 2005.

[76] M. Nielsen, N. Mortensen, M. Albertsen, J. Folkenberg, A. Bjarklev, and D. Bonacinni, "Predicting macrobending loss for large-mode area photonic crystal fibers," *Opt. Express*, vol. 12, no. 8, pp. 1775–1779, 2004.

[77] J. Laegsgaard, N. A. Mortenson, J. Riishede, and A. Bjarklev, "Material effects in air-guiding photonic bandgap fibers," *J. Opt. Soc. Amer. B, Opt. Phys.*, vol. 20, no. 10, pp. 2046–2051, Oct. 2003.

[78] M. Onishi, T. Okuno, T. Kashiwada, S. Ishikawa, N. Akasaka, and M. Nishimura, "Highly nonlinear dispersion-shifted fibers and their application to broadband wavelength converter," *Opt. Fiber Technol.*, vol. 4, no. 2, pp. 204–214, Apr. 1998.

[79] P. Petropoulos, H. Ebendorff-Heidepriem, V. Finazzi, R. Moore, K. Frampton, D. Richardson, and T. Monro, "Highly nonlinear and anomalously dispersive lead silicate glass holey fibers," *Opt. Express*, vol. 11, no. 26, pp. 3568–3573, Dec. 2003.

[80] F. Luan, J. C. Knight, P. St.J. Russell, S. Campbell, D. Xiao, D. T. Reid, B. J. Mangan, D. P. Williams, and P. J. Roberts, "Femtosecond soliton pulse delivery at 800 nm wavelength in hollow-core photonic bandgap fibers," *Opt. Express*, vol. 12, no. 5, pp. 835–840, Mar. 2004.

[81] A. Efimov, A. J. Taylor, F. G. Omenetto, A. V. Yulin, N. Y. Joly, F. Biancalana, D. V. Skryabin, J. C. Knight, and P. St.J. Russell, "Time-spectrally-resolved ultrafast nonlinear dynamics in small-core photonic

crystal fibers: Experiment and modelling," *Opt. Express*, vol. 12, no. 26, pp. 6498–6507, Dec. 2004.

[82] D. G. Ouzounov, F. R. Ahmad, D. Muller, N. Venkataraman, M. T. Gallagher, M. G. Thomas, J. Silcox, K. W. Koch, and A. L. Gaeta, "Generation of MW optical solitons in hollow-core photonic band-gap fibers," *Science*, vol. 301, no. 5604, pp. 1702–1704, Sep. 2003.

[83] J. D. Shephard, J. D. C. Jones, D. P. Hand, G. Bouwmans, J. C. Knight, P. St.J. Russell, and B. J. Mangan, "High energy nanosecond pulses delivered single-mode through hollow-core PBG fibers," *Opt. Express*, vol. 12, no. 4, pp. 717–723, Feb. 2004.

[84] J. D. Shephard, F. Couny, P. St.J. Russell, C. Jones, J. C. Knight, and D. P. Hand, "Improved hollow-core photonic crystal fiber design for delivery of nanosecond pulses in laser micromachining applications," *Appl. Opt.*, vol. 44, no. 21, pp. 4582–4588, Jul. 2005.

[85] L. Michaille, C. R. Bennett, D. M. Taylor, T. J. Shepherd, J. Broeng, H. R. Simonsen, and A. Petersson, "Phase locking and supermode selection in multicore photonic crystal fiber lasers with a large doped area," *Opt. Lett.*, vol. 30, no. 13, pp. 1668–1670, Jul. 2005.

[86] W. J. Wadsworth, R. M. Percival, G. Bouwmans, J. C. Knight, T. A. Birks, T. D. Hedley, and P. St.J. Russell, "Very high numerical aperture fibers," *IEEE Photon. Technol. Lett.*, vol. 16, no. 3, pp. 843–845, Mar. 2004.

[87] W. J. Wadsworth, R. M. Percival, G. Bouwmans, J. C. Knight, and P. St.J. Russell, "High power air-clad photonic crystal fiber laser," *Opt. Express*, vol. 11, no. 1, pp. 48–53, Jan. 2003.

[88] J. Limpert, T. Schreiber, S. Nolte, H. Zellmer, A. Tünnermann, R. Iliew, F. Lederer, J. Broeng, G. Vienne, A. Petersson, and C. Jakobsen, "High-power air-clad large-mode-area photonic crystal fiber laser," *Opt. Express*, vol. 11, no. 7, pp. 818–823, Apr. 2003.

[89] A. Tünnermann, S. Hofer, S. Liem, J. Limpert, M. Reich, F. Roser, T. Schreiber, H. Zellmer, T. Peschel, and V. Guyenot, "Power scaling of high-power fiber lasers and amplifiers," *Laser Phys.*, vol. 15, no. 1, pp. 107–117, 2005.

[90] F. Di Teodoro and C. D. Brooks, "1.1 MW peak-power, 7 W average-power, high-spectral-brightness, diffraction-limited pulses from a photonic crystal fiber amplifier," *Opt. Lett.*, vol. 30, no. 20, pp. 2694–2696, Oct. 2005.

[91] J. Limpert, T. Schriedber, S. Nolte, H. Zellmer, and A. Tünnermann, "All fiber chirped-pulse amplification system based on compression in air-guiding photonic band gap fiber," *Opt. Express*, vol. 11, no. 24, pp. 3332–3337, 2003.

[92] C. J. S. de Matos, J. R. Taylor, T. P. Hansen, K. P. Hansen, and J. Broeng, "All-fiber chirped pulse amplification using highly dispersive air-core photonic band gap fiber," *Opt. Exp.*, vol. 11, no. 22, pp. 2832–2837, 2003.

[93] F. Benabid, F. Couny, J. C. Knight, T. A. Birks, and P. St.J. Russell, "Compact, stable and efficient all-fiber gas cells using hollow-core photonic crystal fibers," *Nature*, vol. 434, no. 7032, pp. 488–491, 2005.

[94] S. G. Leon-Saval, T. A. Birks, N. Y. Joly, A. K. George, W. J. Wadsworth, G. Kakarantzas, and P. St.J. Russell, "Splice-free interfacing of photonic crystal fibers," *Opt. Lett.*, vol. 30, no. 13, pp. 1629–1631, Jul. 2005.

[95] S. G. Leon-Saval, T. A. Birks, J. Bland-Hawthorn, and M. Englund, "Multimode fiber devices with single-mode performance," *Opt. Lett.*, vol. 30, no. 19, pp. 2545–2547, Oct. 2005.

[96] T. A. Birks, G. Kakarantzas, P. St.J. Russell, and D. F. Murphy, "Photonic crystal fiber devices," in *Proc. SPIE—(Fiber-Based Component Fabrication, Testing and Connectorization)*, 2002, vol. 4943, pp. 142–151.

[97] W. J. Wadsworth, A. Witkowska, S. G. Leon-Saval, and T. A. Birks, "Hole inflation and tapering of stock photonic crystal fibers," *Opt. Express*, vol. 13, no. 17, pp. 6541–6549, Aug. 2005.

[98] G. Kakarantzas, T. E. Dimmick, T. A. Birks, R. Le Roux, and P. St.J. Russell, "Miniature all-fiber devices based on CO_2 laser microstructuring of tapered fibers," *Opt. Lett.*, vol. 26, no. 15, pp. 1137–1139, Aug. 2001.

[99] G. Kakarantzas, T. A. Birks, and P. St.J. Russell, "Structural long-period gratings in photonic crystal fibers," *Opt. Lett.*, vol. 27, no. 12, pp. 1013–1015, Jun. 2002.

[100] G. Kakarantzas, A. Ortigosa-Blanch, T. A. Birks, P. St.J. Russell, L. Farr, F. Couny, and B. J. Mangan, "Structural rocking filters in highly birefringent photonic crystal fiber," *Opt. Lett.*, vol. 28, no. 3, pp. 158–160, Feb. 2003.

[101] S. G. Leon-Saval, T. A. Birks, W. J. Wadsworth, P. St.J. Russell, and M. W. Mason, "Supercontinuum generation in submicron fiber waveguides," *Opt. Express*, vol. 12, no. 13, pp. 2864–2869, Jun. 2004.

[102] G. P. Agrawal, *Nonlinear Fiber Optics*, 3rd ed. New York: Academic, 2001.

[103] R. R. Alfano, Ed., *The Supercontinuum Laser Source*, New York: Springer-Verlag, 1989.

[104] S. V. Chernikov, Y. Zhu, J. R. Taylor, and V. P. Gapontsev, "Supercontinuum self-Q-switched ytterbium fiber laser," *Opt. Lett.*, vol. 22, no. 5, pp. 298–300, Mar. 1997.

[105] W. J. Wadsworth, A. Ortigosa-Blanch, J. C. Knight, T. A. Birks, T.-P. M. Man, and P. St.J. Russell, "Supercontinuum generation in photonic crystal fibers and optical fiber tapers—A novel light source," *J. Opt. Soc. Amer. B, Opt. Phys.*, vol. 19, no. 9, pp. 2148–2155, Sep. 2002.

[106] J. M. Dudley, "Review of supercontinuum generation in PCF," *Rev. Mod. Phys.*, 2006. submitted for publication.

[107] I. Hartl, X. D. Li, C. Chudoba, R. Ghanta, T. Ko, J. G. Fujimoto, J. K. Ranka, R. S. Windeler, and A. J. Stentz, "Ultrahigh resolution optical coherence tomography using continuum generation in an air-silica microstructure optical fiber," *Opt. Lett.*, vol. 26, no. 9, pp. 608–610, May 2001.

[108] G. Humbert, W. J. Wadsworth, S. G. Leon-Saval, J. C. Knight, T. A. Birks, P. St.J. Russell, M. J. Lederer, D. Kopf, K. Wiesauer, E. I. Breuer, and D. Stifter, "Supercontinuum generation system for optical coherence tomography based on tapered photonic crystal fibre," *Opt. Express*, vol. 14, no. 4, pp. 1596–1603, Feb. 2006.

[109] R. Holzwarth, J. Reichert, T. Udem, T. W. Hänsch, J. C. Knight, W. J. Wadsworth, and P. St.J. Russell, "An optical frequency synthesizer for precision spectroscopy," *Phys. Rev. Lett.*, vol. 85, no. 11, pp. 2264–2267, Sep. 2000.

[110] H. Hundertmark, D. Wandt, C. Fallnich, N. Haverkamp, and H. Telle, "Phase-locked carrier-envelope-offset frequency at 1560 nm," *Opt. Express*, vol. 12, no. 5, pp. 770–775, Mar. 2004.

[111] S. Coen, A. H. L. Chau, R. Leonhardt, J. D. Harvey, J. C. Knight, W. J. Wadsworth, and P. St.J. Russell, "Supercontinuum generation by stimulated Raman scattering and parametric four-wave mixing in photonic crystal fibers," *J. Opt. Soc. Amer. B, Opt. Phys.*, vol. 19, no. 4, pp. 753–764, Apr. 2002.

[112] W. J. Wadsworth, N. Joly, J. C. Knight, T. A. Birks, F. Biancalana, and P. St.J. Russell, "Supercontinuum generation and four-wave mixing with Q-switched pulses in endlessly single-mode photonic crystal fibers," *Opt. Express*, vol. 12, no. 2, pp. 299–309, 2004.

[113] F. G. Omenetto, N. A. Wolchover, M. R. Wehner, M. Ross, A. Efimov, A. J. Taylor, V. V. Ravi Kanth Kumar, A. K. George, J. C. Knight, N. Y. Joly, and P. St.J. Russell, "Spectrally smooth supercontinuum from 350 nm to 3 μm in sub-centimeter lengths of soft-glass photonic crystal fibers," *Opt. Express*, vol. 14, no. 11, pp. 4928–4934, May 2006.

[114] A. Y. H. Chen, G. K. L. Wong, S. G. Murdoch, R. Leonhardt, J. D. Harvey, J. C. Knight, W. J. Wadsworth, and P. St.J. Russell, "Widely tunable optical parametric generation in a photonic crystal fiber," *Opt. Lett.*, vol. 30, no. 7, pp. 762–764, Apr. 2005.

[115] M. Yu, C. J. McKinstrie, and G. P. Agrawal, "Modulational instabilities in dispersion-flattened fibers," *Phys. Rev. E, Stat. Phys. Plasmas Fluids Relat. Interdiscip. Top.*, vol. 52, no. 1, pp. 1072–1080, Jul. 1995.

[116] J. D. Harvey, R. Leonhardt, K. G. L. Wong, J. C. Knight, W. J. Wadsworth, and P. St.J. Russell, "Scalar modulational instability in the normal dispersion regime using a PCF," *Opt. Lett.*, vol. 28, no. 22, pp. 2225–2227, Nov. 2003.

[117] J. E. Sharping, M. Fiorentino, P. Kumar, and R. S. Windeler, "Optical parametric oscillator based on four-wave mixing in microstructure fiber," *Opt. Lett.*, vol. 27, no. 19, pp. 1675–1677, Oct. 2002.

[118] J. Lasri, P. Devgan, R. Tang, J. E. Sharping, and P. Kumar, "A microstructure-fiber-based, 10-GHz synchronized, tunable optical parametric oscillator in the 1550-nm regime," *IEEE Photon. Technol. Lett.*, vol. 15, no. 8, pp. 1058–1060, Aug. 2003.

[119] Y. Deng, Q. Lin, F. Lu, G. P. Agrawal, and W. H. Knox, "Broadly tunable femtosecond parametric oscillator using a photonic crystal fiber," *Opt. Lett.*, vol. 30, no. 10, pp. 1234–1236, May 2005.

[120] J. G. Rarity, J. Fulconis, J. Duligall, W. J. Wadsworth, and P. St.J. Russell, "Photonic crystal fiber source of correlated photon pairs," *Opt. Express*, vol. 13, no. 2, pp. 534–544, Jan. 2005.

[121] J. Fan, A. Migdall, and L. J. Wang, "Efficient generation of correlated photon pairs in a microstructure fiber," *Opt. Lett.*, vol. 30, no. 24, pp. 3368–3370, Dec. 2005.

[122] J. Fulconis, O. Alibart, W. J. Wadsworth, P. St.J. Russell, and J. G. Rarity, "High brightness single mode source of correlated photon pairs using a photonic crystal fiber," *Opt. Express*, vol. 13, no. 19, pp. 7572–7582, Sep. 2005.

[123] D. V. Skryabin, F. Luan, J. C. Knight, and P. St.J. Russell, "Soliton self-frequency shift cancellation in photonic crystal fibers," *Science*, vol. 301, no. 5640, pp. 1705–1708, Sep. 2003.
[124] N. Y. Joly, F. G. Omenetto, A. Efimov, A. J. Taylor, J. C. Knight, and P. St.J. Russell, "Competition between spectral splitting and Raman frequency shift in negative-dispersion slope photonic crystal fiber," *Opt. Commun.*, vol. 248, no. 1–3, pp. 281–285, Apr. 2005.
[125] P. St.J. Russell, "Light in a tight space: Enhancing matter-light interactions using photonic crystals," in *Proc. Conf. Nonlinear Opt.—(Optical Soc. Amer.)*, 2002, vol. 79, pp. 377–379.
[126] P. St.J. Russell, E. Marin, A. Diez, and A. B. Movchan, "Sonic band gaps in PCF preforms: Enhancing the interaction of sound and light," *Opt. Express*, vol. 11, no. 20, pp. 2555–2560, Oct. 2003.
[127] S. Guenneau and A. B. Movchan, "Analysis of elastic band structures for oblique incidence," *Arch. Ration. Mech. Anal.*, vol. 171, no. 1, pp. 129–150, 2004.
[128] V. Laude, A. Khelif, S. Benchabane, M. Wilm, T. Sylvestre, B. Kibler, A. Mussot, J. M. Dudley, and H. Maillotte, "Phononic band-gap guidance of acoustic modes in photonic crystal fibers," *Phys. Rev. B, Condens. Matter*, vol. 71, no. 4, p. 045107, Jan. 2005.
[129] P. Dainese, P. St.J. Russell, N. Joly, J. C. Knight, G. S. Wiederhecker, H. L. Fragnito, V. Laude, and A. Khelif, "Stimulated Brillouin scattering from multi-GHz-guided acoustic phonons in nanostructured photonic crystal fibres," *Nature Phys.*, vol. 2, no. 6, pp. 388–392, Jun. 2006.
[130] P. Dainese, P. St.J. Russell, G. S. Wiederhecker, N. Joly, H. L. Fragnito, V. Laude, and A. Khelif, "Raman-like light scattering from acoustic phonons in photonic crystal fiber," *Opt. Express*, vol. 14, no. 9, pp. 4141–4150, May 2006.
[131] P. Rabinowitz, A. Stein, R. Brickman, and A. Kaldor, "Efficient tunable hydrogen Raman laser," *Appl. Phys. Lett.*, vol. 35, no. 10, pp. 739–741, Nov. 1979.
[132] L. S. Meng, K. S. Repasky, P. A. Roos, and J. L. Carlsten, "Widely tunable continuous-wave Raman laser in diatomic hydrogen pumped by an external-cavity diode laser," *Opt. Lett.*, vol. 25, no. 7, pp. 472–474, Apr. 2000.
[133] F. Benabid, G. Bouwmans, J. C. Knight, P. St.J. Russell, and F. Couny, "Ultrahigh efficiency laser wavelength conversion in a gas-filled hollow core photonic crystal fiber by pure stimulated rotational Raman scattering in molecular hydrogen," *Phys. Rev. Lett.*, vol. 93, no. 12, p. 123903, 2004.
[134] T. Brabec and F. Krausz, "Intense few-cycle laser fields: Frontiers of nonlinear optics," *Rev. Mod. Phys.*, vol. 72, no. 2, pp. 545–591, Apr. 2000.
[135] A. Paul, R. A. Bartels, R. Tobey, H. Green, S. Weiman, I. P. Christov, M. M. Murnane, H. C. Kapteyn, and S. Backus, "Quasi-phase-matched generation of coherent extreme-ultraviolet light," *Nature*, vol. 421, no. 6918, pp. 51–54, 2003.
[136] S. Ghosh, J. Sharping, D. G. Ouzounov, and A. L. Gaeta, "Resonant optical interactions with molecules confined in photonic band-gap fibers," *Phys. Rev. Lett.*, vol. 94, no. 9, p. 093902, 2005.
[137] F. Benabid, P. S. Light, F. Couny, and P. St.J. Russell, "Electromagnetically-induced transparency grid in acetylene-filled hollow-core PCF," *Opt. Express*, vol. 13, no. 15, pp. 5694–5703, Jul. 2005.
[138] K. Nakajima, K. Hogari, J. Zhou, K. Tajima, and I. Sankawa, "Hole-assisted fiber design for small bending and splice losses," *IEEE Photon. Technol. Lett.*, vol. 15, no. 12, pp. 1737–1739, Dec. 2003.
[139] P. J. Roberts, B. J. Mangan, H. Sabert, F. Couny, T. A. Birks, J. C. Knight, and P. St.J. Russell, "Control of dispersion in photonic crystal fibers," *J. Opt. Fiber Commun. Rep.*, vol. 2, no. 5, pp. 435–461, Nov. 2005.
[140] A. Ashkin, "Acceleration and trapping of particles by radiation pressure," *Phys. Rev. Lett.*, vol. 24, no. 4, pp. 156–159, Jan. 1970.
[141] M. J. Renn, R. Pastel, and H. J. Lewandowski, "Laser guidance and trapping of mesoscale particles in hollow-core optical fibers," *Phys. Rev. Lett.*, vol. 82, no. 7, pp. 1574–1577, Feb. 1999.
[142] M. J. Renn, D. Montgomery, O. Vdovin, D. Z. Anderson, C. E. Wieman, and E. A. Cornell, "Laser-guided atoms in hollow-core optical fiber," *Phys. Rev. Lett.*, vol. 75, no. 18, pp. 3253–3256, Oct. 1995.
[143] F. Benabid, J. C. Knight, and P. St.J. Russell, "Particle levitation and guidance in hollow-core photonic crystal fiber," *Opt. Express*, vol. 10, no. 21, pp. 1195–1203, Oct. 2002.
[144] T. M. Monro, W. Belardi, K. Furusawa, J. C. Baggett, N. G. R. Broderick, and D. J. Richardson, "Sensing with microstructured optical fibres," *Meas. Sci. Technol.*, vol. 12, no. 7, pp. 854–858, Jul. 2001.
[145] P. M. Blanchard, J. G. Burnett, G. R. G. Erry, A. H. Greenaway, P. Harrison, B. J. Mangan, J. C. Knight, P. St.J. Russell, M. J. Gander, R. McBride, and J. D. C. Jones, "Two-dimensional bend sensing with a single, multi-core optical fiber," *Smart Mater. Struct.*, vol. 9, no. 2, pp. 132–140, 2000.
[146] W. N. MacPherson, J. D. C. Jones, B. J. Mangan, J. C. Knight, and P. St.J. Russell, "Two-core photonic crystal fiber for Doppler difference velocimetry," *Opt. Commun.*, vol. 223, no. 4–6, pp. 375–380, Aug. 2003.
[147] W. N. MacPherson, E. J. Rigg, J. D. C. Jones, V. V. Ravi Kanth Kumar, J. C. Knight, and P. St.J. Russell, "Finite-element analysis and experimental results for a microstructured fiber with enhanced hydrostatic pressure sensitivity," *J. Lightw. Technol.*, vol. 23, no. 3, pp. 1227–1231, Mar. 2005.
[148] P. J. A. Sazio, A. Amezcua-Correa, C. E. Finlayson, J. R. Hayes, T. J. Scheidemantel, N. F. Baril, B. R. Jackson, D.-J. Won, F. Zhang, E. R. Margine, V. Gopalan, V. H. Crespi, and J. V. Badding, "Microstructured optical fibers as high-pressure microfluidic reactors," *Science*, vol. 311, no. 5767, pp. 1583–1586, Mar. 2006.

Philip St.J. Russell (M'05) received the M.A. and D.Phil. degrees from the University of Oxford, Oxford, U.K., in 1976 and 1979, respectively.

He subsequently worked as a Humboldt Fellow at the Technische Universität Hamburg, Hamburg, Germany; IBM, Yorktown Heights, NY; University of Nice, Nice, France; University of Southampton, Southampton, U.K.; and University of Kent, Kent, U.K. He holds the Alfried Krupp von Bohlen und Halbach Chair for Experimental Physics and is the Director of the Max-Planck Research Group for Optics, Information, and Photonics, University of Erlangen-Nuremberg, Erlangen, Germany. From 1996 to 2005, he was a Professor with the Department of Physics, University of Bath, Bath, U.K., where he founded and led the Photonics and Photonic Materials Group (now the Centre for Photonics and Photonic Materials). Since 1977, he has specialized in the behavior of light in periodic structures as well as nonlinear optics, waveguides, and optical fibers. He was the founder of the startup company BlazePhotonics Ltd. (April 2001 to August 2004), whose aim was the development and commercial exploitation of photonic crystal fiber. He has over 600 publications and is the holder of 37 patents in many aspects of photonics.

Dr. Russell is a Fellow of the Optical Society of America. In 2000, he won the Optical Society of America's Joseph Fraunhofer Award/Robert M. Burley Prize for the invention of photonic crystal fiber, which he first proposed in 1991. He is the founding Chair of the Optical Society of America's Topical Meeting Series on Bragg Gratings, Photosensitivity, and Poling in Glass. In 2002, he won the Applied Optics Division Prize of the U.K. Institute of Physics. In 2004, he received the Royal Society/Wolfson Research Merit Award. In 2005, he won the Thomas Young Prize of the Institute of Physics. In May 2005, he was elected Fellow of the Royal Society, and in September, he received the 2005 Körber Prize for European Science at a ceremony in Hamburg. He was an IEEE-LEOS Distinguished Lecturer from 2004 to 2006.